3.3: Diapycnal mixing processes in the ocean interior

Jennifer MacKinnon
Scripps Institution of Oceanography
La Jolla, CA USA

Lou St. Laurent
Woods Hole Oceanographic Institution
Woods Hole, MA USA

Alberto Naveira Garabato
National Oceanography Centre
University of Southampton, UK

Draft created March 11, 2013

Abstract

Diapycnal mixing in the ocean interior is driven by a wide range of processes, each with distinct governing physics and unique global geography. Here we review the primary processes responsible for turbulent mixing in the ocean interior, with an emphasis on active work from the past decade. We conclude with a discussion of global patterns of mixing and their importance for regional and large-scale modeling accuracy.

Contents

1

1. Introduction

Physical processes in the ocean span a vast range of spatial and temporal scales. The winds, tides and atmospheric buoyancy forcing of the ocean are processes that occur over horizontal scales of O(100–1000km), driving basin-scale gyres, the meridional overturning circulation, and wave motions such as Kelvin, Rossby and internal waves. A range of dynamical processes ultimately lead to viscous dissipation at small scales, both at ocean boundaries and in the interior of the deep ocean. The resultant turbulent mixing plays a primary role in the thermodynamic balance of the ocean.

Much of the past half-century of research has revolved around attempts to reconcile global estimates of how much turbulent mixing is needed to explain observed water property distributions, or to close global energy budgets, with mixing rates inferred from small-scale observations. In a simplistic two-dimensional view, the meridional overturning circulation (MOC) consists of cold water sinking at the poles and upwelling at lower latitudes as it is slowly warmed by heat turbulently diffusing down from the surface. Matching the rate of diapycnal upwelling to rates of deep water production at high latitudes gives the canonical average required diapycnal eddy diffusivity of 1×10^{-4} m^2 s^{-1} below the main thermocline (*Munk*, 1966; *Munk and Wunsch*, 1998). In a related calculation *Munk and Wunsch* (1998) and *Wunsch and Ferrari* (2004) argue that approximately 2 TW of power is required to replenish potential energy at the rate it is released by the the MOC itself. *St. Laurent and Simmons* (2006) demonstrate that there is a rough equivalence between the total oceanic dissipation by turbulence and the power required estimates for the ocean interior. The main candidates for external energy sources are the wind and the tides, which together approximately supply the needed power channeled largely but not entirely through the internal-wave field (Sec. 4.1).

The original Munk paper touched off an observational search for the canonical 10^{-4} m^2 s^{-1} diffusivity that has lasted decades. Initial reports of diffusivities a factor of 10 lower than the Munk value (*Gregg*, 1987; *Ledwell et al.*, 1998) gave rise to the impression that we were ‘missing’ mixing, a notion that is still pervasive. As one offshoot of the supposed discrepancy, a vein of reasoning was developed that much of the MOC could be closed adiabatically through wind-driven Ekman suction and upwelling in the Southern Ocean (*Toggweiler and Samuels*, 1998; *Marshall and Radko*, 2006; *Wolfe and Cessi*, 2010; *Nikurashin and Vallis*, 2011). In this view turbulent mixing was needed only at the deepest levels of the ocean, with an associated much lower power requirement.

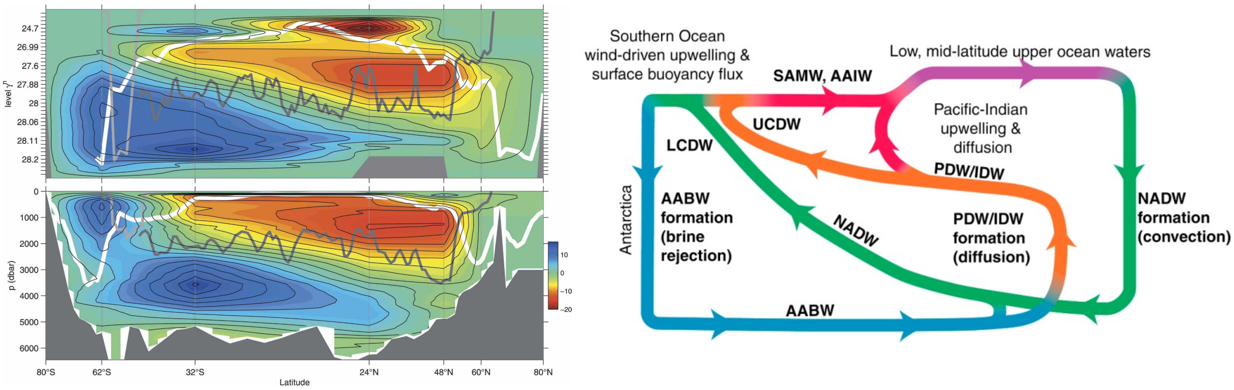

Figure 1: Left panels: zonally averaged stream functions for the global meridional overturning circulation in density (top) and pressure (bottom) coordinates, every 2 Sv contoured. Typical winter mixed-layer densities/ depths (white), the mean depth of ocean ridge crests (dark gray), and the depth of the Scotia Arc east of Drake Passage (light gray) are also shown. Reproduced from *Lumpkin and Speer* (2007). Here it appears that the NADW and AABW form distinct overturning cells. Right: schematic of three-dimensional global overturning circulation, reproduced from *Talley et al.* (2011). Here it is clear that diapycnal mixing, particularly in the Pacific and Indian Oceans, plays a fundamental role in the upwelling that ultimately returns deep and bottom waters towards the surface.

However, more recent evidence suggests the quest for missing mixing may be a red herring, for several reasons. First, there is often a depth mis-match in the discussion. The original Munk calculation was for water *deeper than 1 kilometer*, below the main thermocline, while the observations by *Gregg* (1987) and *Ledwell et al.* (1998) were in or above the main thermocline. The bulk of microstructure observations of mixing taken below the main thermocline in fact do show values on the order of 10^{-4} m^2 s^{-1} or larger (*St. Laurent and Simmons* (2006); *Waterhouse et al.* (2013) and Sec. 5.2). Second, a preponderance of inverse models and related calculations demonstrate that average diffusivites of $1-10\times10^{-4}$ m^2 s^{-1} are required at all depths below the main thermocline to close mass or tracer budgets in individual ocean basins (e.g. *Ganachaud and Wunsch*, 2000; *Talley et al.*, 2003; *Lumpkin and Speer*, 2007). Many of these estimates are for domains that do not include the Southern Ocean.

Finally, the two-dimensional, zonally averaged view of the MOC can hide essential pathways of water transformation. In a zonally averaged view, it appears that there are two somewhat distinct overturning cells, one involving North Atlantic Deep Water (NADW) sinking in the North Atlantic and upwelling in the Southern Ocean, and the second involving Antarctic Bottom Water (AABW) sinking near Antarctica and upwelling slowly into the bottom of the upper cell. However, the three-dimensional circulation appears to be more like a mobius strip, in which the majority of NADW does not directly return to the North Atlantic after upwelling in the Southern Ocean, but cools and sinks as AABW. The majority of the AABW diabatically upwells into intermediate water in the Indian and Pacific Oceans, and then returns to the surface through a combination of diabetic and adiabatic processes (*Lumpkin and Speer*, 2007; *Talley et al.*, 2011; *Talley*, 2013). The process is illustrated schematically in Figure 1. From this Lagrangian perspective, most water parcels on the so-called 'conveyor belt' gain buoyancy through diapycnal mixing below the main thermocline at some point during their journey.

There currently appears to be rough agreement between the power required to drive the overturning circulation, the power available to the internal wave field, and the global sum of observed mixing rates, with all estimates around 2-3 TW (*Wunsch and Ferrari*, 2004; *St. Laurent and Simmons*, 2006; *Ferrari and Wunsch*, 2009). Given the sparse nature of microstructure observations, narrowing the comparison down further is a daunting task. Instead, a major emphasis over the last decade has been on process studies targeted at understanding specific dynamical regimes, with the hope that such understanding could then be extrapolated globally (Sec. 5.2). At the same time, the combination of increasing sophistication and decreasing spurious diffusion in large-scale numerical models has shown that circulation and tracer distributions are extremely sensitive not just to the average value of diapycnal diffusivity but to its detailed geographical distribution (Sec. 5.3; *Griffies et al.*, 2010). Because the global energy budget of ocean mixing has been well-reviewed elsewhere (*Munk and Wunsch*, 1998; *Wunsch and Ferrari*, 2004; *St. Laurent and Simmons*, 2006; *Kuhlbrodt et al.*, 2007; *Ferrari and Wunsch*, 2009), the bulk of this chapter is dedicated to describing the wide range of dynamic processes responsible for creating turbulence in the ocean interior and the associated complex geography of diapycnal mixing.

Though much of the global energetics discussion revolves around deep and abyssal mixing rate, there has also been increasing interest in diapycnal mixing in the top few hundred meters of the ocean. Elevated upper ocean diffusivity is especially important in tropical regions, where it can significantly influence mixed-layer heat content and associated air-sea heat fluxes. So before moving on to the zoo of deep ocean processes we first briefly review recent developments in our understanding of upper ocean turbulence.

Our review is far from comprehensive. We neglect a number of major areas relevant to a discussion of ocean mixing that have recently been reviewed elsewhere. This includes the topic of double diffusion (*Schmitt*, 2012), which is known to be important in many regions, such as the tropical Atlantic (*Schmitt et al.*, 2005), and the Arctic (*Timmermans et al.*, 2003). We also neglect the area of biogenic turbulence, concerning turbulence levels generated by the kinetic activities of marine animals (*Dewar et al.*, 2006; *Young*, 2012). The classic turbulence problem of the bottom boundary layer is also ignored, despite recent interest especially in coastal oceanography (e.g., *Perlin et al.* (2005)). In addition, the role of non-linearities in the equation of state for seawater is not discussed here (*Klocker and McDougall*, 2010). Finally, turbulent entrainment in deep overflows, essential for setting the water mass characteristics of all deep and bottom waters of the worlds oceans, is nicely reviewed by *Legg* (2012) and discussed in Chapter 3.6 of this volume.

2. Mixing Basics

Throughout we are primarily concerned with mixing resulting from small scale three-dimensional turbulence. Molecular diffusion of heat and salt is a slow process, characterized by diffusivities of order 1.4×10^{-7} m^2 s^{-1} and 1.5×10^{-9} m^2 s^{-1} respectively (*Gill*, 1982). Turbulent stirring of fluid acts to dramatically increase gradients and accelerate the rate of irreversible mixing. Such mixing increases the potential energy of stratified water. The associated turbulent fluxes are often characterized by an effective or turbulent diffusivity. A commonly used formulation relates the diapycnal diffusivity to the turbulent dissipation rate, ϵ, a common measure of the strength of turbulence, through an assumed mixing efficiency,

$$\kappa_\rho = \Gamma \frac{\epsilon}{N^2} \tag{1}$$

where in practice the mixing efficiency is often taken to be $\Gamma = 0.2$ (*Osborn*, 1980). In reality, Γ is likely to vary with the background stratification and the strength of the turbulence (*Shih et al.*, 2005; *Ivey et al.*, 2008), but a discussion of these issues is beyond the purview of the present chapter. Interested readers are referred to recent reviews by *Staquet and Sommeria* (2002), *Ivey et al.* (2008), *Moum and Rippeth* (2009) and *Hughes et al.* (2009). Here we specify the strength of observed mixing rates using both the turbulent dissipation rate (typical values of 10^{-10} to 10^{-9} W kg^{-1} in the deep ocean) and the turbulent diapycnal diffusivity (often just referred to as the diffusivity, with typical values of 10^{-5} to 10^{-4} m^2 s^{-1}), depending on the metric used in the original studies being referenced.

Turbulence in the ocean may be produced through a range of instabilities, details of which are reviewed by *Smyth and Moum* (2001); *Wunsch and Ferrari* (2004); *Thorpe* (2005); *Ivey et al.* (2008). Away from the direct influence of surface fluxes, turbulence is often related to vertical shear or convective instabilities (*Alford and Pinkel*, 2000; *Smyth and Moum*, 2012). The tendency for a fluid to undergo shear instability is controlled by the gradient Richardson number, $Ri = N^2/S^2$, which reflects the counteracting stabilizing and destabilizing effects of stratification and shear. Many models include a turbulent diffusivity that is a function of the Richardson number, but it is only applied to vertically coarse and generally low-frequency shear features that are well resolved by the model (Sec. 5.3). Observations and process studies described below demonstrate that most turbulence in the ocean interior is produced by small-scale or high frequency motions that are not generally resolved by global or even regional scale models, and are unlikely to be resolved in the foreseeable future. Hence there is a premium on understanding the nature and geography of the dynamics driving turbulent mixing, so that it may be properly parameterized. Our focus is not on the details of the turbulence per se, but on the larger scale dynamics that set the stage and supply the energy for turbulent mixing, largely by moving energy to small vertical scales where shear is large.

Observationally, the most direct way to measure turbulent mixing is through purposeful dye release (*Ledwell et al.*, 1993, 2000, 2011), a complicated endeavor. The turbulent dissipation rate may be estimated using microstructure instruments that measure either velocity or scalar fluctuations within the inertial subrange that characterizes turbulence on the smallest scales, typically centimeters or smaller (*Moum et al.*, 1995; *Gregg*, 1998; *Lueck et al.*, 2002). These estimates are accurate, but the instruments are specialized and difficult to operate. The turbulent dissipation rate may also be estimated from measurements of the outer scales of turbulent overturns, typically meters, which may be made from a variety of instruments. Moving to even larger scales, recent techniques have allowed the strength of turbulence to be inferred from measurements of internal waves, whose breaking is presumed to produce the turbulence. Such finescale methods are described in Section 5.1.

3. Turbulence in and below the surface mixed layer

Diapycnal mixing processes in the upper ocean are an important component of the coupled climate system. The ocean surface boundary layer is the subject of vigorous interactions with the overlying atmosphere and cryosphere. Heat, fresh water, and momentum are exchanged across the ocean surface at large rates, and upper-ocean water mass properties are modified by turbulent processes. A striking feature of the upper ocean (and one that is defining of ocean circulation) is the glaring contrast between the energy flow across the ocean surface and that through the base of the mixed layer into the stratified ocean below. Of the approximately 65 TW of power that have been estimated to be imparted to the ocean surface by the wind, less than 5% are thought to be transmitted to the ocean interior (*Huang*, 1998; *Wunsch and Ferrari*, 2004; *Ferrari and Wunsch*, 2009). Since surface fluxes are well reviewed elsewhere (*Large and Nurser* (2001) and Chapter 3.1 of this volume), here we focus on the processes through which surface fluxes may be transmitted into the ocean interior through turbulent mixing at and below the mixed-layer base. Just below the mixed layer a strongly stratified 'transition layer' mediates the transfer of heat, nutrients, and dissolved gasses to the deeper ocean (*Johnston and Rudnick*, 2009). Turbulence in the transition layer is driven primarily by a combination of shear extending down below the mixed layer, penetrative convection, and breaking high-frequency internal waves. Mixed-layer deepening by direct wind forcing and convection are represented in existing bulk formula (*Price et al.*, 1986; *Large et al.*, 1994; *Moum and Smyth*, 2001). Here we describe a few processes that are areas of active research and are not represented in most mixed-layer parameterizations.

3.1. Langmuir turbulence

Langmuir turbulence occurs when a surface boundary layer is forced by wind in the presence of surface waves. The combination drives elongated counter-rotating vortices organized into the wave direction (*McWilliams et al.*, 1997), generally thought to be caused by an instability arising from the interaction of the Stokes drift induced by the surface waves and the shear of the upper-ocean flow (*Craik and Leibovich*, 1976; *Sullivan et al.*, 2004; *McWilliams et al.*, 2004). Even though the Stokes drift is confined to a shallow vortex layer on the order of the significant wave height deep, downwelling jets originating within that layer penetrate well beyond it (*Polton and Belcher*, 2007). Because of these jets, the influence of surface waves may be felt, via Langmuir turbulence, throughout the depth of the mixed layer. It has been suggested, in fact, that Langmuir turbulence may be more effective than shear-driven turbulence in deepening the mixed layer (*Skyllingstad and Denbo*, 1995).

The importance of Langmuir turbulence and its significance in inducing diapycnal mixing in the upper ocean are commonly assessed by reference to the turbulent Langmuir number $La_t = (u_*/u_{s0})^{1/2}$, where u_* is the surface friction velocity in the water and u_{s0} is the surface Stokes drift (*McWilliams et al.*, 1997; *Li et al.*, 2005). Langmuir turbulence becomes a dominant process when $La_t \leq 0.3 - 0.5$, whereas shear-driven turbulence is dominant for significantly higher La_t (e.g. *Li et al.*, 2005; *Grant and Belcher*, 2009). Climatological estimates of La_t suggest that mixing in the ocean surface boundary layer is often dominated by Langmuir turbulence (*Li et al.*, 2005; *Belcher et al.*, 2012). Crucially, the mixing associated with Langmuir cells can not be parameterized by local closures schemes and requires an alternate approach. More details of Langmuir cell dynamics and parameterization are nicely reviewed by *Sullivan and McWilliams* (2010).

3.2. Inertial motions

Another mechanism via which wind forcing may destabilize a one-dimensional upper ocean is the generation of inertial motions. As a natural resonant frequency of the system, inertial motions in the surface mixed layer are efficiently forced by time variable wind stresses, in particular those with strong inertially rotating components such as due to passing mid-latitude storms. The generation process is often modeled using the damped-slab model of *Pollard and Millard* (1970)[see also *D'Asaro* (1985)], which describes the temporal evolution of inertial oscillations in a one-dimensional mixed layer of constant depth as a balance between wind forcing and a parameterized (linear) damping. Integrated estimates of power going into near-inertial motions derived from global wind products range from 0.3 to 1.2 TW (*Alford*, 2001; *Watanabe and Hibiya*, 2002; *Jiang et al.*, 2005), and are highly sensitive to the specific wind products used, as well as assumptions about the damping rate of near-surface oscillations (*Plueddemann and Farrar*, 2006). Physically, the damping rate represents energy loss both through shear instabilities at the base of the mixed layer (*Crawford and Large*, 1996; *Skyllingstad et al.*, 2000) and radiation of near-inertial internal waves (Sec. 4.1.2). The damped-slab model has been tuned to produce estimates of upper-ocean inertial velocity that are in good qualitative correspondence with observations, given values of the damping coefficient in the range 2 to 10 days (*D'Asaro et al.*, 1995). The geography of near-inertial motion generation varies seasonally, but generally follows storm tracks. Near-inertial waves and associated mixing are a key component of the ocean response to hurricanes (*Price et al.*, 2008). The global patterns of power input into inertial motions calculated using a slab model approach bear many similarities to the geography of near-surface near-inertial kinetic energy measured from surface drifter tracks (Fig. 3). Convergences and divergences of inertial motions pump energy into the ocean interior in the form of internal waves, which are considered further in Section 4.1.2.

3.3. An equatorial example

Much of the recent observational progress in understanding turbulent mixing in the transition layer comes from equatorial studies, where dynamics are further complicated by the presence of the strongly sheared equatorial undercurrent. Regional and global ocean models show that coupled air-sea phenomena like ENSO are quite sensitive to mixing in the transition layer, as the rate of downward heat flux out of the mixed layer affects SST (*Harrison and Hallberg*, 2008). An example of the rich field of turbulence present beneath the equatorial mixed layer is shown in Figure 2. The turbulent dissipation rate (bottom panel) shows bursts of turbulence extending well below the mixed layer (upper black line) on most nights, with separate patches of turbulence at times present at the upper edge of the equatorial undercurrent (lower black line). Bursts of high-frequency oscillations penetrating below the mixed layer have been well documented at the equator (visible in the middle panel in Fig. 2 for example), though they likely occur elsewhere as well (*Lien et al.*, 2002). A variety of theories have been proposed to explain observed high-frequency motions in this depth range, from generation by shear instabilities acting on the upper edge of the equatorial undercurrent (*Moum et al.*, 2011; *Smyth et al.*, 2011), to internal waves triggered by nocturnal convection bursts impinging on the stratified mixed-layer base (*Gregg et al.*, 1985; *Wijesekera and Dillon*, 1991), to the obstacle effect as Langmuir cells or other undulations of the mixed-layer base are advected by mixed-layer currents over the stratified layer below (*Polton et al.*, 2008). The spate of recent equatorial mixing observations also highlights the compounding effects of processes with very different timescales. For example, while the bursts of turbulence visible in Figure 2 clearly have a diurnal pattern, *Moum et al.* (2009) demonstrate that slow modulation by passing tropical instability waves is enough to nudge the underlying undercurrent shear past the threshold for shear instability, with resultant turbulent mixing

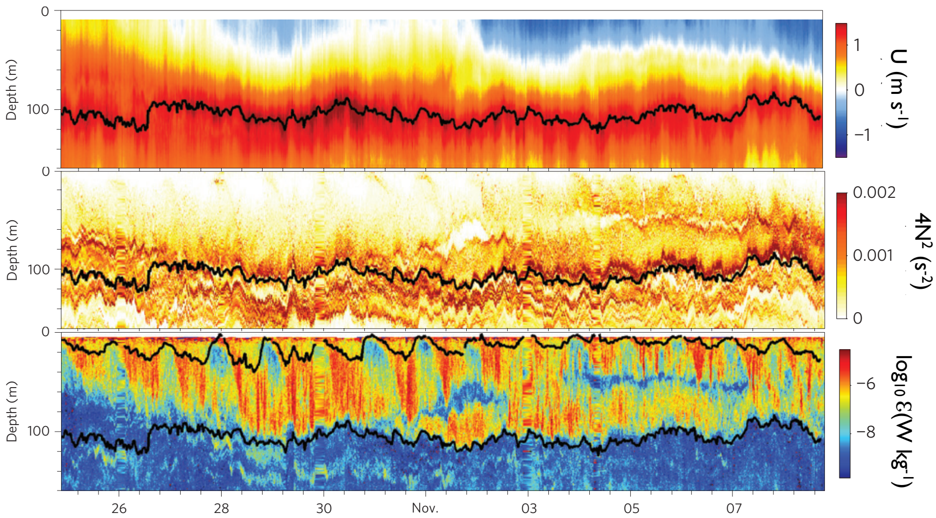

Figure 2: The rich structure of near-surface turbulence. Profiling time series at 0°,140° W in boreal autumn 2008, reproduced from *Moum et al.* (2009). (top) Zonal velocity: the core (eastward velocity maximum) of the eastward-flowing EUC is shown as a black line; (middle) $4N^2$; (lower) turbulence dissipation rate, ϵ. The mixed layer is defined by the upper black line in e as the depth at which ρ deviates by 0.01 kg m^{-3} from its surface value.

large enough to be an order-one player in local vertical heat budgets. While questions remain as to the dynamics driving transition layer mixing at the equator (or elsewhere), it is becoming increasingly clear that large-scale modeled upper ocean budgets and air-sea fluxes are sensitive to how these effects are parameterized (Sec. 5.3).

3.4. Fronts and other lateral processes

While mixing near the surface of the ocean is often discussed and parameterized as a one-dimensional process, the phenomenology of mixing is greatly enriched in the presence of significant lateral density gradients. The widespread occurrence of such gradients on horizontal scales down to 1 to 2 km throughout the oceans extratropics has been demonstrated by observations with towed instrumentation (*Rudnick and Ferrari*, 1999; *Hosegood et al.*, 2006; *Capet et al.*, 2008), and has also been suggested by numerical simulations of the ocean's submesoscale (e.g. *Lapeyre et al.*, 2006; *Capet et al.*, 2008; *Fox-Kemper et al.*, 2008). The results of such simulations are consistent with an interpretation of the observed submesoscale lateral density structure as arising from fast-growth (growth rate of ~f), small-scale (lateral scale on the order of 1 km) ageostrophic baroclinic instabilities (e.g. *Stone*, 1966, 1970; *Molemaker et al.*, 2005; *Boccaletti et al.*, 2007) of mixed-layer fronts, which result in an adiabatic restratification of the upper ocean. The mixed-layer fronts are thought to be formed by strong convective mixing induced by atmospheric forcing (followed by a rapid relaxation of lateral density gradients to geostrophy through Rossby adjustment; e.g., *Tandon and Garrett* (1995)) or, more commonly, by the straining of the large-scale horizontal density distribution by the mesoscale eddy field (*Treguier et al.*, 1997; *Fox-Kemper et al.*, 2008; *Ferrari et al.*, 2008, 2010). At any rate, it is now recognized that the upper-ocean density field is fundamentally three-dimensional, and that this can qualitatively alter the effects of wind and buoyancy forcing on turbulent dissipation and diapycnal mixing in the upper ocean.

Evidence for the latter statement has proliferated in recent years. For example, numerical simulations of buoyancy-driven convection at a mixed-layer front (e.g. *Taylor and Ferrari*, 2010) reveal that, whilst classical upright convection (in which the turbulent buoyancy flux supplies the production of turbulent kinetic energy) occurs in a relatively shallow upper layer, the bulk of the depth range affected by the forcing experiences symmetric instability, a gravitational centrifugal form of instability undergone by gravitationally stable fluid with negative potential vorticity in which shear production (by perturbations growing along isopycnals) is the primary source of turbulent kinetic energy (e.g. *Thorpe and Rotunno*, 1989; *Haine and Marshall*, 1998). Similarly, wind forcing of a mixed-layer front has been shown to have qualitatively distinct impacts on the upper ocean relative to the one-dimensional mixed-layer scenario that is traditionally considered. Upfront wind forcing (i.e. oriented in the direction opposite to the quasi-geostrophic flow of the surface ocean) induces an Ekman flow directed toward the dense side of the front, and thereby restratifies the upper ocean (e.g. *Thomas*, 2005; *Thomas and Ferrari*, 2008; *Mahadevan et al.*, 2010).

Resonant wind forcing by upfront winds has been found to provide a particularly rapid and effective mechanism for injecting near-inertial internal waves into the stratified upper ocean (*Forryan et al.*, 2013).Downfront wind forcing, in turn, de-stratifies the upper ocean and promotes turbulent dissipation and diapycnal mixing. The means by which it does so centrally involves symmetric instability (*Taylor and Ferrari*, 2010; *Thomas and Taylor*, 2010). Since kinetic energy is extracted by the instability from the geostrophic flow and ultimately dissipated in small-scale turbulence, wind-forced symmetric instability leads to a significant reduction of the wind work that is available for increasing the kinetic energy of the ocean's general circulation (*Thomas and Taylor*, 2010), and can produce rates of upper-ocean turbulent dissipation and diapycnal mixing that greatly exceed expectations from wind-forced boundary layer theory (*D'Asaro et al.*, 2011).

In regions of strong frontogenesis, ageostrophic secondary circulation may also strongly interact with internal gravity waves, transferring energy through them towards turbulent dissipation at small scales (*Thomas*, 2012). Finally, it has been argued that turbulent dissipation and diapycnal flow in the upper ocean may be induced by the interaction of the mesoscale eddy field with the ocean surface, which forces eddy buoyancy fluxes to be directed horizontally (i.e. diapycnally) in the mixed layer (*Treguier et al.*, 1997; *Radko and Marshall*, 2004; *Ferrari et al.*, 2008). The coupling of mesoscale eddy stirring with air-sea heat fluxes can also act to reduce variance in near-surface tracer fields (*Shuckburgh et al.*, 2011).

4. Mixing in the ocean interior

Diapycnal mixing in the ocean interior fluxes heat, salt and dissolved gasses across density classes and influences the slowly evolving meridional overturning circulation. Away from direct influence of the surface or bottom boundaries, power to supply turbulent mixing must be imported into the ocean interior, largely through the propagating internal waves that produce most observed shear. Mixing may also occur near the ocean floor and the resultant mixed fluid can spread out along isopycnals into the interior. Here, we provide a basic review of some of the processes acting to drive mixing well below the mixed layer. This is followed by a discussion of processes driving mixing in the Southern Ocean (Sec. 4.4), which have a flavor all of their own.

4.1. Internal wave breaking

Internal-wave breaking has long been argued to be the dominant source of turbulent mixing away from boundary layers. Energy is added into the internal-wave field primarily by the tides and winds, producing internal tides and near-inertial internal waves, respectively. In regions of very strong near-bottom flows, internal waves may also be created by a lee-wave mechanism, an example of which will be presented in Section 4.4. In both tide- and wind-forced internal waves, power input into the ocean is often dominated by energy flux into relatively large-scale internal waves, with vertical wavelengths from hundreds to thousands of meters (*Gill*, 1984; *St. Laurent and Garrett*, 2002) (Fig. 3). However, dissipation results from the breaking of small-scale waves (generally tens of meters or less) through shear or convective instabilities (*Alford and Pinkel*, 2000; *Staquet and Sommeria*, 2002). The geography of internal-wave mixing thus is controlled by the combination of the generation geography, wave propagation and refraction, and processes that move energy towards smaller, more dissipative scales of motion.

4.1.1. Dissipation near internal-tide generation sites

Internal tides are generated in areas where the barotropic tide (diurnal or semidiurnal) sloshes over rough or steep topography, the process of which is reviewed by *St. Laurent and Garrett* (2002) and *Garrett and Kunze* (2007). Global patterns of internal tide generation reflect the product of barotropic tidal strength and topographic roughness, and resemble maps of deep-sea energy loss from the barotropic tide (*Egbert and Ray*, 2001; *Jayne and St. Laurent*, 2001; *Simmons et al.*, 2004b). Globally there is approximately 1 TW of power going into internal tides (*Wunsch and Ferrari*, 2004). Recent work has conceptually divided the problem into nearfield and farfield components representing, respectively, the fates of comparatively higher-mode waves that break near the generation region and low-mode waves that propagate away.

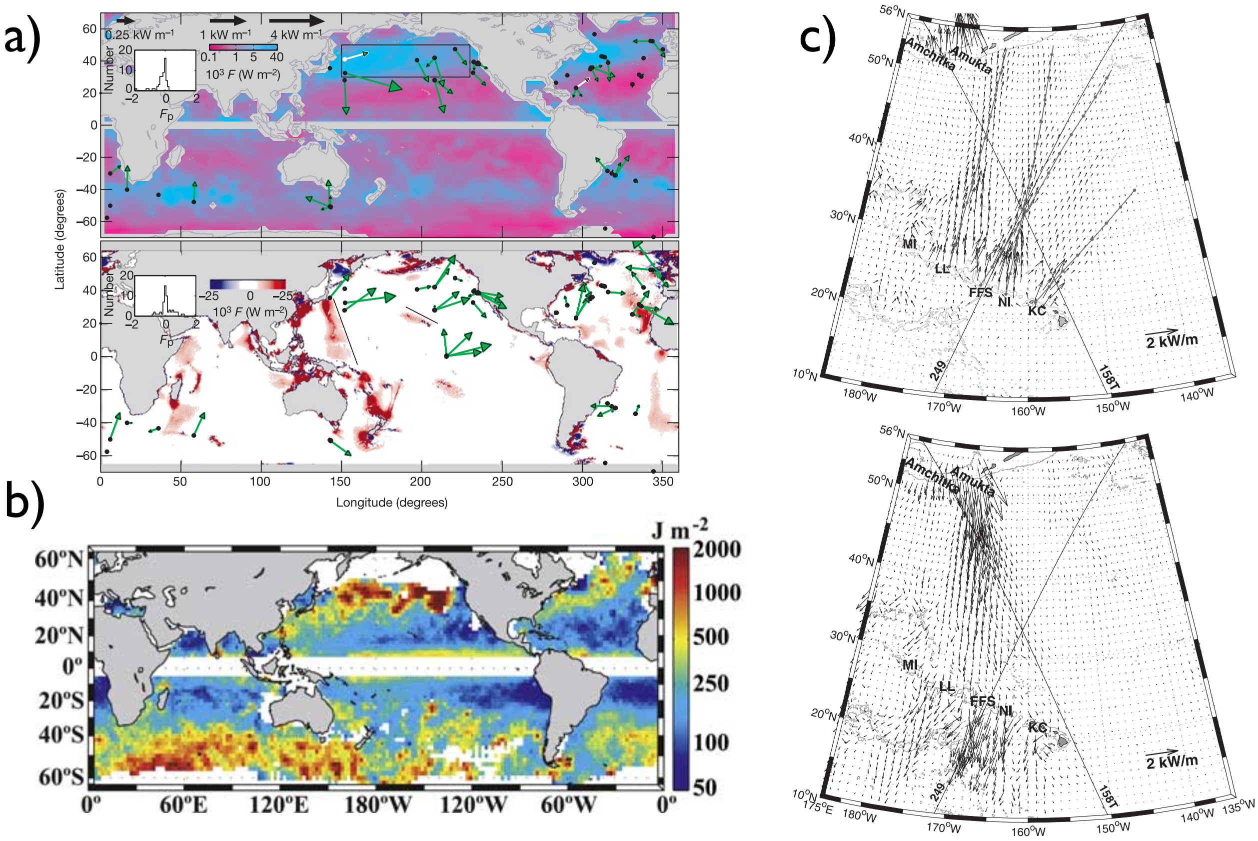

Figure 3: Global patterns of internal wave generation and propagation. a) Power going into near-inertial motions at the ocean surface (top) and internal tides (bottom), from *Alford* (2003). Arrows represent near-inertial and internal tide energy fluxes as measured at available historical moorings. b) Depth-integrated near-inertial kinetic energy in the surface mixed layer as estimated from surface drifter tracks (*Chaigneau et al.*, 2008). c) Mode-1 Internal tide energy fluxes in the North Pacific estimated from satelite altimetry, decomposed into northward and southward components (*Zhao and Alford*, 2009)

The nearfield part of tidal dissipation has been well studied observationally in the last two decades. For example, the Hawaii Ocean Mixing Experiment (HOME) (*Klymak et al.*, 2006) and the Brazil Basin Experiment (*Polzin et al.*, 1997) both find turbulence elevated by orders of magnitude within several horizontal wavelengths (hundreds of km or less) of internal-tide generation sites. There are a range of processes responsible. Strong flow over steep slopes can produce very strong mixing driven by a combination of convective instabilities, breaking internal lee waves, and hydraulic jumps. Recent work in the very energetic Luzon Strait showcases the range of phenomenology possible (*Alford et al.*, 2011; *Pinkel et al.*, 2012; *Klymak et al.*, 2012). Slightly further aloft, higher-mode wave-like motions may achieve critical Froude numbers leading to strong breaking, a process observed in HOME (*Klymak et al.*, 2008) and the subject of recent modeling and theoretical parameterization attempts (*Legg and Klymak*, 2008; *Klymak et al.*, 2010a). Dissipation rates are also elevated in high-mode beam-like structures seen in some observations (*Lien and Gregg*, 2001; *Martin et al.*, 2006; *Cole et al.*, 2009; *Johnston et al.*, 2011), models (*Gerkema et al.*, 2006) and laboratory experiments (*Peacock et al.*, 2008).

Turbulence may be elevated near rough topography even apart from influence of such direct tidally forced nonlinearities. For example, over the deep rough topography of the eastern Brazil Basin, turbulent dissipation is elevated for several kilometers above the bottom, with a magnitude that steadily decreases with increasing height (*Polzin et al.*, 1997). *Polzin* (2009) suggests that the pattern is set by the rate at which an upward propagating quasi-linear internal tide steadily loses energy through weakly nonlinear wave-wave interactions to higher-mode waves, which in turn have higher shear and dissipate locally. The hypothesis is roughly consistent with the empirical formulation proposed by *St. Laurent et al.* (2002) and the analytical formulation of *Polzin* (2004) now being implemented in large-scale models (Sec. 5.3). In this case, and perhaps in similar environments of deep rough topography, measurements are consistent with most of the energy going into the internal tide being dissipated locally, that is within a few hundred kilometers (*Polzin*, 2004; *Waterhouse et al.*, 2013).

Yet in other locations, particularly over tall steep topography, the majority of generated internal tide energy escapes to propagate up to thousands of kilometers across ocean basins in the form of low-mode internal waves. Evidence for these propagating waves can be seen in satellite altimetry (*Zhao and Alford*, 2009), in situ flux measurements (*Alford*, 2003; *Althaus et al.*, 2003; *Rudnick et al.*, 2003; *Alford et al.*, 2007; *Zhao et al.*, 2010), and high-resolution models (*Simmons*, 2008). (Fig. 3c). The ultimate fate of this energy is less clear: some is bled into the ambient internal wave field through nonlinear wave-wave interactions producing the 'background' diffusivity of the main thermocline and abyss (Sec. 4.1.3), one subset of which is Parametric Subharmonic Instability (PSI), some may become trapped in mesoscale shear or vorticity, and the remainder likely scatters over deep ocean topography or breaks on distant continental slopes (Sec. 4.1.4).

4.1.2. Dissipation near inertial-wave generation sites

Though near-inertial internal waves provide one of the most prominent peaks in any oceanic energy spectrum, comprising half the kinetic energy in the internal wave field and a larger percentage of the shear, remarkably little is known about their generation, evolution or decay (*Ferrari and Wunsch*, 2009). Generation mechanisms include wind forcing at the ocean surface, loss of balance of mesoscale or submesoscale features (Sec. 4.3), or nonlinear interactions between other internal waves (*McComas and Müller*, 1981). At the ocean surface, time variable wind stresses force inertial motions in the surface mixed layer, since the inertial frequency is the natural 'ringing' frequency of any fluid on a rotating planet (Sec. 3.2). Horizontal convergences and divergences of this moving mixed-layer water at the edges of the forced region create vertical velocities with an inertial period at the mixed-layer base, which in turn force near-inertial internal waves in the stratified region below. The horizontal wavelength of the propagating waves is heavily influenced by the beta effect, namely that for a patch large enough to feel the latitudinal change of inertial frequency motions at the northern end of the patch gradually get out of phase with those near the southern end. Inertial motions are also sensitive to mesoscale vorticity, which can add or detract from the planetary vorticity to change the effective inertial frequency felt by these motions. Detailed dynamics of the generation and initial propagation are described by *D'Asaro* (1985); *D'Asaro et al.* (1995); *Young and Ben-Jelloul* (1997); *Moehlis and Llewellyn-Smith* (2001). Simple models predict that most of the energy goes into low-mode internal waves (*Gill*, 1984; *Zervakis and Levine*, 1995). However, the higher, shear-containing modes are also of interest as they may provide a more direct pathway to mixing.

As with the internal tide, some of the wind-generated energy probably dissipates in the upper ocean, particularly that of higher-mode waves (*Alford and Gregg*, 2001), leading to maps of estimated upper ocean diffusivities (e.g. Fig. 7b) that mirror patterns of mixed-layer near-inertial energy in Fig. 3. Such upper-ocean dissipation likely has a seasonal cycle (*Jing and Wu*, 2010; *Whalen et al.*, 2012). High-mode near-inertial internal waves are particularly sensitive to interactions with mesoscale vorticity, making associated patterns of mixing very sensitive to ambient conditions (*Rainville and Pinkel*, 2004; *Danioux et al.*, 2008; *Elipot et al.*, 2010) .

Yet substantial wind-generated near-inertial energy is also clearly reaching the deep sea, as evidenced by a deep seasonal cycle of near-inertial energy (*Mihaly et al.*, 1998; *Alford and Whitmont*, 2007; *van Haren*, 2007; *Silverthorne and Toole*, 2009) and direct observations of downward energy flux. *Alford et al.* (2012) observe up to a third of near-inertial power input into the surface mixed layer of the North Pacific transiting vertically through 800-meters depth. Low-mode near-inertial waves can also be observed propagating equatorward from the mid-latitude storm track (*Alford* (2003), Fig. 3). The ultimate fate of these waves, like that of propagating low-mode internal tides, is unknown. Several candidates for dissipation of low-mode internal waves are discussed in the following subsections.

One of the persistent mysteries regarding near-inertial internal waves is the presence of large numbers of waves with properties suggesting upward propagating group velocities (e.g *Alford*, 2010). Most of the shear resides in waves with small vertical wavelengths and associated very slow vertical propagation speeds, making bottom reflection of surface generated waves of this wavelength an unlikely possibility. Some types of wave-wave interactions (Sec. 4.1.3) and loss of mesoscale balance (Sec. 4.3) may also produce upward propagating near-inertial waves, although the rates and pathways are somewhat unclear. Given that turbulent mixing is intricately related to small-scale shear and that near-inertial motions are the largest source of small-scale shear, improving our understanding of these processes seems essential.

4.1.3. Wave-wave interactions

A leading candidate for energy loss from propagating internal waves is nonlinear interactions with an ambient internal wave field. Wave-wave interactions redistribute energy to a variety of frequencies and wavenumbers. The broad-band internal wave continuum displays a remarkably narrow range of spectral shapes (*Polzin and Lvov*, 2011), presumably reflecting attractive states for the underlying nonlinear dynamics (*Müller et al.*, 1986; *Lvov et al.*, 2010). Within the continuum, there is a general tendency for energy to flow towards higher vertical wavenumbers, where it is likely to lead to wave breaking and dissipation (*McComas and Müller*, 1981; *Lvov et al.*, 2010) (Sec. 5.1).

Propagating low-mode tidal or near-inertial internal waves may bleed energy through the continuum, creating essentially a smeared out wake of dissipation along wave propagation paths. In turn, the energy lost from low-mode waves likely supplies and maintains the continuum, with regional differences in continuum shape reflecting features of the primary forcing wave (*Polzin and Lvov*, 2011). While documenting the relationship between continuum energy levels and mixing rates is an important step, the ability to predict the resultant global patterns of turbulent mixing requires a prognostic relationship between available tidal or near-inertial internal wave energy, the continuum it supplies, and the eventual rate of small-scale wave breaking (*Polzin*, 2009).

Parametric subharmonic instability (PSI) is a specific type of wave-wave interaction that transfers energy from a low-mode wave to two high-mode waves near half the frequency. The interaction can occur anywhere where the subharmonic waves are within the internal wave band ($f \leq \omega \leq N$), but may be particularly efficient where the submarmonic is equal to the local inertial frequency (*Hibiya et al.*, 2002; *MacKinnon and Winters*, 2003, 2005; *Furuichi et al.*, 2005; *Nikurashin and Legg*, 2011) For the semi-diurnal tide, this occurs near a latitude of 29N/S. Numerical studies predict significantly elevated mixing at these latitudes (*MacKinnon and Winters*, 2005; *Simmons*, 2008) with some suggestively corroborating observational evidence (*Hibiya and Nagasawa*, 2004). However, a major field campaign to track the internal tide northward from Hawaii found only a moderate effect near 29N, with diffusivity in the upper ocean elevated by a factor of 2-4 over background levels. The discrepancy between observations and the more catastrophic numerical results is likely due to the complex and time-variable nature of the internal tide in that region (*Alford et al.*, 2007; *Hazewinkel and Winters*, 2011; *MacKinnon et al.*, 2013). Other studies have found evidence of PSI of strong internal tides at lower latitudes (*Carter and Gregg*, 2006), of the diurnal internal tide near 14 N (*Alford*, 2008), and of equatorward-propagating near-inertial internal waves between 5° and 15° N (*Nagasawa et al.*, 2000).

4.1.4. Distant graveyards

The remainder (perhaps the majority) of propagating low-mode internal-wave energy scatters to higher modes and dissipates due to interaction with topography. Some of this interaction may occur with mid-basin topographic features (*Gilbert and Garrett*, 1989; *Lueck and Mudge*, 1997; *Toole et al.*, 1997; *Müller and Liu*, 2000; *Johnston et al.*, 2003). Altimetric evidence suggests that in basins like the North Pacific, with relatively smooth bottom topography, the majority of low-mode internal tide energy propagates virtually unscathed for thousands of kilometers (*Ray and Mitchum*, 1996, 1997; *Zhao and Alford*, 2009). Care must be taken in interpreting patterns of tidal fluxes such as Figure 3c, as some of the apparent decay in altimetric fluxes may be due to loss of coherence as waves refract in an evolving mesoscale (rending them invisible to this detection technique) rather than genuine dissipation. Comparable observations of long-range propagating low-mode near-inertial wave patterns are not available. Much of this low-mode energy may dissipate where waves scatter and reflect off continental slopes and shelves. Simple theory predicts that an internal wave hitting a near-critical slope (one with the same angle from vertical as the ray path of the incident wave) will reflect into smaller-scale waves that are more likely to break (*Eriksen*, 1985, 1998; *Ivey et al.*, 2000; *McPhee-Shaw and Kunze*, 2002; *Nash et al.*, 2004; *Kelly and Nash*, 2010). The details of such processes are poorly constrained by existing observations but likely are sensitive to both the steepness and the three-dimensional roughness of the slope in question. For example, *Klymak et al.* (2010b) observed that a substantial portion of mode-one tidal energy impinging on a supercritical slope in the South China Sea reflects back as low-mode waves, while the remainder propagates onshore as a dissipative bore. In contrast, incoming internal tides hitting rough Oregon slope were observed to shoal, refract, and break (*Martini et al.*, 2011; *Kelly et al.*, 2011). Canyons littered along continental slopes may also focus incoming waves (*Kunze et al.*, 2002; *Gregg et al.*, 2011), and canyon mixing may contribute significantly to basin-wide averages (*Kunze et al.*, 2012). Open questions here include what percentage of the total available internal tide energy dissipates where waves hit the continental slope, how that mixing is distributed both laterally along the global coastline and vertically, and how efficiently such boundary mixing communicates with the interior. As an example of the later issue, *Garrett* (1991, 2001) point out that the reduction of mixing efficiency near the bottom (essentially because you are mixing already mixed water) renders extrapolation of boundary mixing values to basin-wide averages a somewhat tricky endeavor.

4.2. Mixing in fracture zones

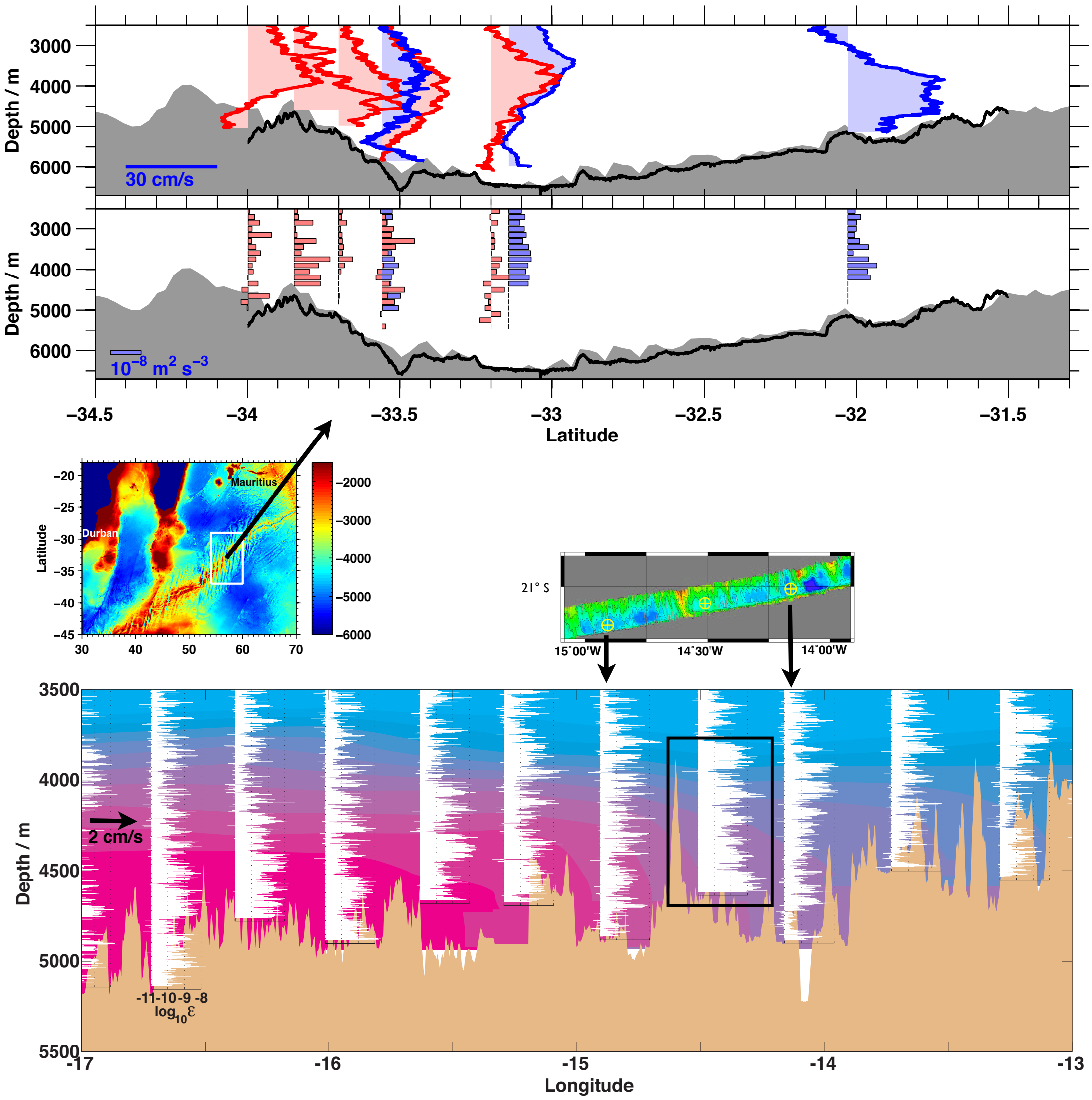

Figure 4: Strong mixing in fracture zones. Upper plots are sections along the Atlantis II Fracture Zone. Along-axis velocity profiles are from *MacKinnon et al.* (2008) and a CLIVAR 2009 repeat transect (J. Swift, G. Johnson, pers. comm.) shown in the upper sub-panel in blue and red, respectively, and the corresponding dissipation rate estimates in the lower sub-panel. Lower panel: multibeam bathymetry of the unnamed FZ canyon studied by *St.Laurent et al.* (2001) and *Thurnherr et al.* (2005). The locations of 3 microstructure profiles are shown upstream, just downstream, and further downstream of a prominent sill (boxed area). Potential temperature layers are indicated by the color shading in the background. Turbulent dissipation rates (W/kg) are shown, with reference axis indicated on the profile on the left.

Measurements of very strong rates of turbulent mixing in deep fracture zones (FZ) place them on a short list for globally significant mixing hotspots. One of the most well studied sites is the Romanche Fracture Zone in the equatorial Atlantic, where velocity, hydrographic and microstructure measurements have been taken (e.g. *Polzin et al.*, 1996a; *Ferron et al.*, 1998). There, some of the largest abyssal turbulence levels ever observed were measured ($\epsilon > 10^{-5}$ W kg^{-1}), resulting from the strong northward flow of Antarctic Bottom Water descending over a series of sills. Spatial patterns in the turbulence associated with flow through the Romanche FZ suggest that a significant portion of the observed energy dissipation is associated with hydraulic jumps occurring at several sills. While the total area of elevated mixing is small, *Polzin et al.* (1996b) argue the net impact in terms of diapycnal buoyancy flux is equivalent to a diffusivity of 10^{-5} m^2 s^{-1} acting over a 1.5×10^6 km^2 region.. The Romanche FZ thus stands as perhaps the single most important water mass conversion pathway for AABW in the Atlantic (*Bryden and Nurser*, 2003). Elevated levels of mixing have also been inferred at the Samoan Passage, an analogous 'choke point' for bottom water entering the Pacific (*Roemmich et al.*, 1996). Exceptionally strong turbulent mixing associated with accelerated sill flows within the Samoan Passage was recently confirmed by direct microstructure observation (Alford, Carter and Girton, pers. comm. 2012).

Similarly strong mixing was observed in the Atlantis II FZ, which is the main passageway for northward flow of Lower Circumpolar Deep Water and Antarctic Bottom Water across the Southwest Indian Ridge into the main Indian Ocean Basin (*Donohue and Toole*, 2003). *MacKinnon et al.* (2008) measure a net 3 Sv northward transport of deep and bottom water. They estimate dissipation rates and diffusivities up to and above 10^{-3} m^2 s^{-1} in the bottom two kilometers of the water column, in and below the main northward jet (Fig. 4). Unlike the Romanche measurements, the *MacKinnon et al.* (2008) measurements were taken well downstream of the entrance sill and hence the observed mixing is likely not due to hydraulic effects (although other data suggest hydraulic features are likely present up-stream). Instead, the pattern of increasing diffusivity with depth was consistent with an observed increase in finescale shear with depth (likely due to internal waves), above the background level expected by the Garrett and Munk canonical spectrum. They hypothesize that the shear associated with the mean flow may provide critical layers to enhance internal-wave breaking.

Turbulence and mixing levels at several other smaller FZs have also been studied. This includes an unnamed FZ along Mid-Atlantic Ridge of the Brazil Basin (*St.Laurent et al.*, 2001), where high spatio-temporal measurements indicated evidence for mixing by externally forced turbulence (i.e., with an energy source other than the near-bottom flow alone). In the case of the Brazil Basin, the depth-integrated dissipation rates were observed to modulate with the spring-neap cycle (*St.Laurent et al.*, 2001). This modulation was not observed in the near-bottom turbulence levels alone, ruling out that the signal was caused by frictional processes or mixing near sills, but instead pointing to the internal tide as a mechanism for providing a source of turbulence into the abyssal interior. *Thurnherr et al.* (2005) examined the details of the turbulent events observed in the Brazil Basin FZs, and found that within the canyons, the largest dissipation levels were likely related to flows that had accelerated over sills (Fig. 4). Their analysis suggests that sill-related mixing contributes at least as much to the diapycnal buoyancy flux in the canyon as tidally forced internal-wave breaking.

Other mid-ocean ridge features, such as those associated with rift valleys, have also been found to be characterized by strong near-bottom flows and elevated turbulence levels. The Lucky Strike site of the Mid-Atlantic Ridge (*St.Laurent and Thurnherr*, 2007) is a narrow passage feature within the rift valley. There, the largest near-bottom dissipation rates were again associated with hydraulically controlled flow over sills. As was the case in the Romanche FZ, dissipation rates as large as $\epsilon = 10^{-5}$ W kg^{-1} were found to characterize the area just down-stream of the sill, with associated diffusivities of 3×10^{-2} m^2 s^{-1} . But unlike the Romanche FZ, which sits at nearly 5000-m depth, the Lucky Strike site is at 2000-m, allowing the elevated turbulence levels there to provide mixing at the level of the North Atlantic Deep Water (NADW) Given the exceptional levels of turbulence and mixing at Lucky Strike, *St.Laurent and Thurnherr* (2007) suggest that in bulk such sites may be significant contributors to basin averaged diapyncal mixing of mid-depth water masses like NADW. Based on an analysis of bathymetric data for the region between 20N and 60N, they speculate that flow through rift valley passages may contribute up to 50% of the mixing along the 2000-m depth-level in this region. Given the relative dearth of measurements in such 'commonplace' fracture zones, their relative contribution to total mixing for deep isopycnals, and the ultimate power source for this mixing, remain important open questions.

4.3. Mesoscale dissipation as a source of turbulent mixing

The global mesoscale energy budget is surprisingly uncertain. Energy is input into large-scale motions primarily by the winds, with a global integral around 1 TW (*Ferrari and Wunsch*, 2009). Resultant large-scale currents decay through baroclinic or other instabilities into mesoscale eddies. *Wunsch and Ferrari* (2004) and *Ferrari and Wunsch* (2009) discuss several candidate mechanisms that may dissipate mesoscale energy, including bottom drag, loss of balance into ageostrophic motions, generation of internal lee waves, and suppression by wind work. Each of these mechanisms could potentially dissipate between 0.1 and 1 TW. The relative importance of each of these processes, and the associated amount of turbulent mixing produced by each, is as yet unclear. Some evidence points to enhanced dissipation in western boundary currents (*Zhai et al.*, 2010). Several examples of ageostrophic dissipation processes in the upper ocean are discussed in Section 3.4, while two mechanisms relevant to the deep ocean are described below.

Internal lee wave generation provides a complementary mechanism to internal tide generation to explain observed enhanced turbulent dissipation rates over rough topography. The impingement of the oceans quasi-geostrophic circulation on small-scale (with characteristic horizontal scales of 1-10 km) topographic roughness may represent a globally significant source of internal waves. *Scott et al.* (2011) and *Nikurashin and Ferrari* (2011) provide independent estimates of the global rate of internal wave generation by quasi-geostrophic flow over topography and find it to be in the range of 0.2 to 0.5 TW, i.e. between approximately 25% and 60% of the wind work on the oceans general circulation and the rate of mesoscale eddy generation by baroclinic instability (*Wunsch and Ferrari*, 2004; *Ferrari and Wunsch*, 2009). However, some recent evidence suggests these techniques may be significant over-estimates (K. Polzin, pers. comm.). The Southern Ocean is the area of strongest predicted lee-wave generation, as will be discussed in Section 4.4. Related work by *Dewar and Hogg* (2010) demonstrate that when geostropically balanced features interact with topography a suite of unbalanced motions can result, many associated with enhanced turbulent dissipation.

Direct interaction between mesoscale eddies and internal waves in the stratified interior of the ocean may represent another important pathway from the mesoscale to turbulent mixing. Yet there are few theories and even fewer observations of the process. Common types of interaction discussed in the literature include an internal wave propagating in a sheared flow that encounters a critical layer (*Winters and D'Asaro*, 1994; *Kunze et al.*, 1995) or internal waves trapped in the lowered effective vorticity of a horizontally sheared flow (*Kunze*, 1985; *Rainville and Pinkel*, 2004). Both of these phenomena involve wave refraction in relatively simple symmetric mean flows without substantial transfer of energy from the mesoscale flow to internal waves. In contrast, recent work by *Buhler and McIntyre* (2005) and *Polzin* (2010) consider the more general case of a fully three-dimensional mesoscale flow. They show that in a mesoscale flow with significant horizontal strain, internal waves can strongly refract and become trapped, a situation *Buhler and McIntyre* (2005) dub 'wave capture'. Conceptually, a wavepacket of almost any initial wavenumber orientation will rotate to align with the axis of maximum strain, and phase lines will be squeezed together in a similar way to contours of a passive scalar. Both horizontal and vertical wavenumbers exponentially grow until the wave presumably breaks. *Polzin* (2010) shows suggestive observational evidence in support of this theory, and describes the effective viscous drag on the mesoscale as characterized by a horizontal viscosity of 50 $\mathrm{m^2\,s^{-1}}$. *Ferrari and Wunsch* (2009) globally extrapolate Polzin's results to produce a net mesoscale power loss of 0.35 TW, with most of the resultant diapycnal mixing presumably taking place in the upper kilometer of the ocean in regions of high mesoscale kinetic energy, consistent with some of the findings of *Whalen et al.* (2012). *Thomas* (2012) point out that in environments with order 1 Rossby number (e.g. frontal regions), secondary circulations arise with make the nature of the nonlinear interaction more complex.

4.4. In depth example: Southern Ocean mixing

Both *Scott et al.* (2011) and *Nikurashin and Ferrari* (2011) highlight the Southern Ocean as the most prominent region of internal lee wave generation in the world ocean (Sec. 4.3). There, the deep-reaching, multi-jet Antarctic Circumpolar Current (ACC) flows over small-scale topographic roughness associated with numerous ridges and plateaus in each of the major ocean basins. The consequent internal wave activity in the form of lee waves has been inferred in measurements of velocity finestructure downstream of the Kerguelen Plateau (*Polzin and Firing*, 1997) and in the Scotia Sea (*Naveira Garabato et al.*, 2004). At each of these sites, finestructure evidence suggested the turbulence levels were substantially enhanced due to the breaking of internal lee waves. High rates of diapycnal mixing for the Southern Ocean as a whole have been suggested by inverse studies of the circulation (*Heywood et al.*, 2002; *Lumpkin and Speer*, 2007; *Zika et al.*, 2009), with deep-ocean average diffusivity levels of $\kappa_\rho \sim O(10^{-4}\ \mathrm{m^2\,s^{-1}})$. However, these estimates are indirect, being based mainly on mass balance or the structure of the large-scale thermohaline fields.

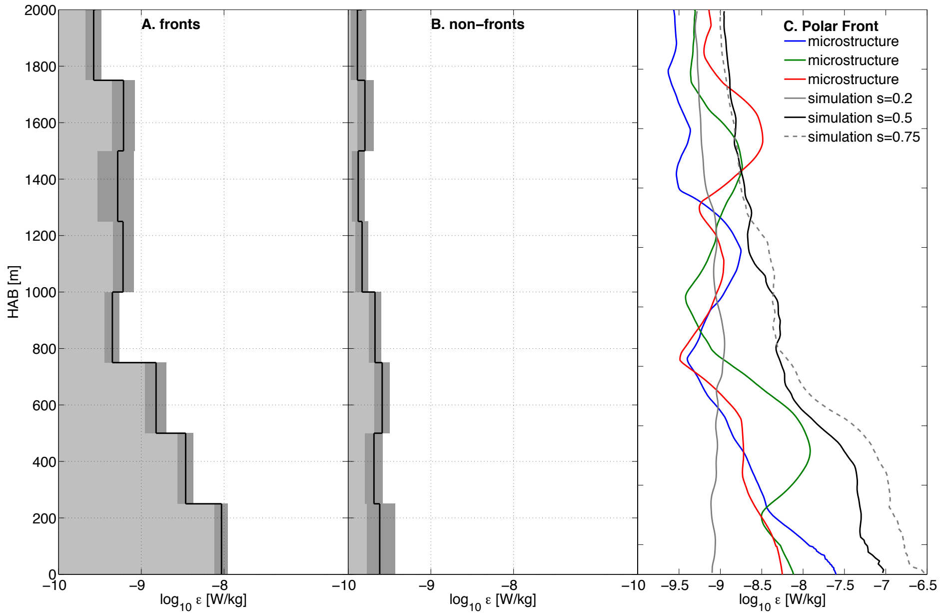

Figure 5: Average height-above-bottom (HAB) profiles of turbulent kinetic energy dissipation rates of frontal (A) and non-frontal regions (B) as estimated from the microstructure data from Drake Passage surveys done at and just upstream of the Phoenix Ridge (St. Laurent et al., 2012). These represent ensemble means using 250-m HAB bins from approximately 12 profiles each. In each bin, the line denotes the mean, and the shading about the mean indicates the 95% confidence interval. Lighter grey shading fills the gap between the estimates and the oceanic background dissipation rate level of 10^{-10} W kg^{-1} . Individual turbulent dissipation rate profiles (colored curves) and numerical simulations (*Nikurashin and Ferrari* (2010); gray curves) from the Polar Front above the Phoenix Ridge are also shown (C). Measured profiles span the Polar Front from south (blue) to north (red). The numerical simulations were done using several values of a steepness parameter (s) found to characterize the finescale steepness of the ridge topography, and hence the spectral character of the generated lee waves.

More targeted studies have examined the Kerguelen Plateau and the Southeast Pacific / Southwest Atlantic sectors of the Southern Ocean, where the ACC flows around and over complex topography, with direct measurements of internal waves and turbulence. *Waterman et al.* (2013a) present the first microstructure measurements in the ACC, in the context of the Kerguelen Plateaus northern flank. They find a systematic enhancement of dissipation rates above background levels ($\epsilon \sim 10^{-9}$ W kg^{-1}) in the upper 1000-1500 m of the water column, and elevated dissipation and mixing rates ($\epsilon \sim 10^{-9}$ W kg^{-1} , $\kappa \sim 10^{-4}$m^2 s^{-1}) in deep-ocean sites where the ACC jets impinge on complex small-scale topography. In several of these cases there is a noticeable discrepancy between microstructure and finescale parameteriztions of dissipation that may be related to the dynamics of wave-mean-flow interaction (Sec. 5.1).

Finestructure estimates in the Drake Passage include those described by *Naveira Garabato et al.* (2004), who inferred very large dissipation and diffusivity levels throughout the Drake Passage. However, other studies using the same parameterization as part of larger-scale Southern Ocean (*Sloyan*, 2005) and global ocean (*Kunze et al.*, 2006) examinations inferred somewhat more modest Drake Passage mixing levels, with local enhancements generally confined to depths below 1500 m. Some of the discrepancy can be attributed to difference in implementation of the finescale parameterization (Sec. 5.1). In the case of *Sloyan* (2005), the enhanced mixing levels were concentrated into the frontal zones. Another Drake Passage study, *Thompson et al.* (2007), focused on the upper 1000 m of the water column and examined vertical overturns implied by inversions in temperature and density profile data from expendable instruments (XCTDs and XBTs). That work reported diffusivity levels implied by Thorpe Scales (*Dillon*, 1982) reaching $\kappa = 10^{-3}$m^2 s^{-1} , and a strong seasonal cycle to the mixing.

The first direct measurements of turbulence levels in the Drake Passage were made in 2010 as part of the Diapycnal and Isopycnal Mixing Experiment in the Southern Ocean (DIMES). DIMES is a joint tracer release and microstructure sampling experiment, focused on examining the spatial variation in mixing levels as a mid-depth tracer cloud evolves as it passes from the Pacific through the Drake Passage into the Scotia Sea (*Ledwell et al.*, 2011). During the first year of the experiment, the tracer injected on the 27.9 $\mathrm{kg\,m^{-3}}$ neutral density surface evolved from a very small highly concentrated patch to an O(1000 km) cloud in the Pacific sector just upstream of Drake Passage. The vertical (diapycnal) diffusivity acting in the cloud was $\kappa = 1.3 \times 10^{-5}\mathrm{m^2\,s^{-1}}$, consistent a mean dissipation level of $10^{-10}\mathrm{W\,kg^{-1}}$ measured by microstructure sampling. These mixing levels are the same order of magnitude as background mixing in the mid-latitude thermocline, and seem to suggest elevated mixing in the Southern Ocean is not as wide spread as some previous studies have predicted.

Within Drake Passage, measurements were also made near the Phoenix Ridge. This mid-ocean ridge site is the first of a series of significant topographic regions that the ACC passes on its eastward path into the Atlantic. Measurements described by *St. Laurent et al.* (2012) show enhanced levels of turbulence in the frontal zones (Fig. 5a). Turbulent dissipation rates exceed 1×10^{-8} $\mathrm{W\,kg^{-1}}$ at heights-above-bottom (HAB) reaching 1000-m, supporting diffusivities from 1×10^{-4} to 1×10^{-3} $\mathrm{m^2\,s^{-1}}$. These elevated mixing rates decay to background rates above 2000 m, suggesting that the energy in the deep internal wave field is locally driving turbulence only to mid-depth. Outside of the frontal zones, turbulence levels show no enhancement (Fig. 5b), indicating that without a deep-reaching current, there is no mechanism to generate lee waves. In the specific case of the Polar Front at the Phoenix Ridge, observed turbulent dissipation rates and depth structure show some similarity to the numerical simulations of *Nikurashin and Ferrari* (2010) (Fig. 5c). They found near-bottom inertial oscillations accompany the generation of lee waves, leading to instability and enhanced dissipation near the bottom. Dissipation profiles from the simulations (black and grey curves, shown for simulations according to internal wave/topographic steepness ratios (s)) show similar depth dependent structures to measured profiles in frontal zones (left panel), with the general decay of dissipation levels with height. However, the magnitude of the *Nikurashin and Ferrari* (2010) prediction appears to be a significant overestimate (Fig. 5 and *Waterhouse et al.* (2013)).

While most turbulent dissipation measurements are limited to the Austral summer season, inferred diffusivities calculated from EM-APEX floats (*Ledwell et al.*, 2011) and repeat hydrography (*Thompson et al.*, 2007) show mixing rates are somewhat elevated in the winter. Given that the strength of the near-bottom flow incident on bathymetric features appears to be the most critical indicator of mixing intensity via lee-wave processes, eddy variability of the ACC may dictate the temporal variability of mixing in the deep Southern Ocean rather than seasonal forcing. Year-long moorings deployed as part of the DIMES experiment are just being retrieved as of this writing - analysis of that data over the next few years will hopefully shed some light on the dynamics and variability of energetic mixing in the Drake Passage specifically and the Southern Ocean more generally.

5. Discussion

5.1. Finescale parameterizations of turbulent mixing

Over the last two decade a ‘finescale parameterization’ of turbulent dissipation and diffusivity has been developed that combines observations of internal wave energy levels with theoretical models of turbulence as controlled by wave-wave interaction rates (Sec. 4.1.3; *Polzin et al.*, 1995; *Gregg et al.*, 2003; *Kunze et al.*, 2006; *Polzin et al.*, 2013). As this method has gained increasingly widespread use in recent years, we feel it deserves a few comments here. The basic idea is that in a steady state the rate of downscale energy transfer through a broadband internal wave continuum by wave-wave interactions can be equated to the dissipation rate at small scales. The rate of downscale energy transfer can be estimated using properties of internal wave strain or shear measured at vertical scales of order 10 to 100 meters, raising the tantalizing possibility that mixing in the ocean could be observed (however crudely) using a much larger variety of instruments than specialized microstructure sensors.

Most formulations are based on the empirically derived Garrett-Munk (GM) vertical wavenumber spectra of internal wave shear and strain, both of which are nearly white (flat) at larger scales, then drop off with a -1 slope beyond a cutoff wavenumber (k_c in Figure 6) (*Gregg and Kunze*, 1991). Physically, motions at scales larger than the cutoff (smaller wavenumbers) are interpreted as weakly nonlinear internal waves, while motions at smaller scales become more strongly nonlinear, eventually leading to wave breaking (*D’Asaro and Lien*, 2000). For the empirically derived GM spectrum, the transition occurs at a wavelength of $2\pi/k_c = 10$ m. For other observations, the cutoff appears to move towards lower wavenumbers with higher spectral energy levels (*Gargett*, 1990). *Polzin et al.* (1995) interpret this as the internal wave field maintaining a constant Richardson number, which is related to the wave-turbulence transition point suggested by *D’Asaro and Lien* (2000).

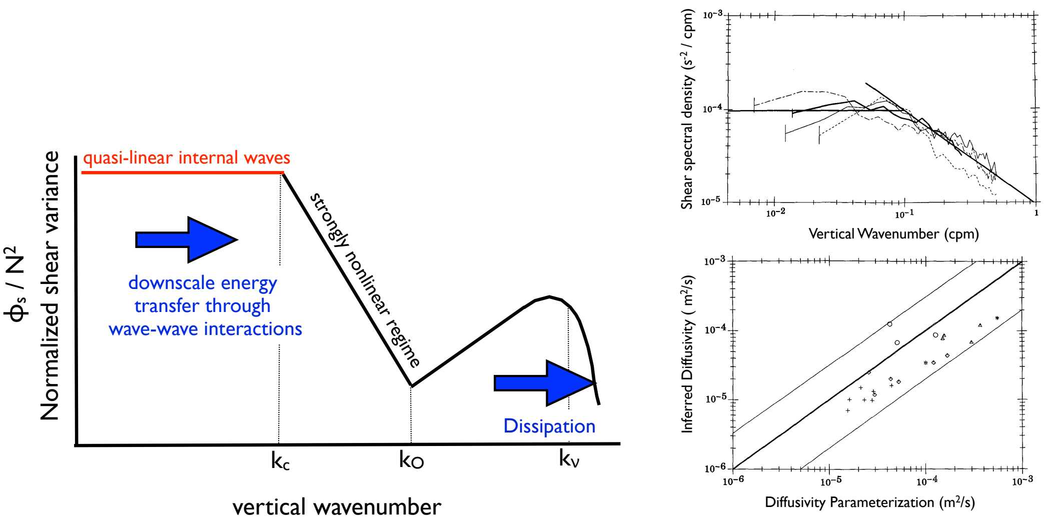

Figure 6: Left: Sketch of idealized vertical wavenumber spectra of stratification normalized shear showing steady-state spectral shapes for the internal wave regime (low wavenumbers / large vertical scales), the transition range, and the turbulent subrange at high wavenumbers / small vertical scales. Wavenumbers indicated on the x-axis correspond to the Kolmogorov scale (k_v), the Ozmidov scale (k_O), and the edge of the quasi-linear internal wave regime (k_c). The blue arrows schematically indicate the direction of energy transfer from large to dissipative scales. Right: several observed vertical wavenumber spectra (upper) and comparison of diffusivity inferred from the finescale method to that inferred from microstructure data (lower). Right panels are reproduced from *Polzin et al.* (1995).

The rate of downscale energy transfer through the weakly nonlinear range, and thus the dissipation rate, tends to scale quadratically with the spectral level ($\hat{E}$), a scaling consistent between theory (*McComas and Müller*, 1981; *Müller et al.*, 1986; *Henyey et al.*, 1986; *Lvov et al.*, 2004), observations (*Gregg*, 1989; *Polzin et al.*, 1995; *Gregg et al.*, 2003), and numerical simulations (*Winters and D'Asaro*, 1997). *Henyey et al.* (1986) physically interpret this transfer rate as the rate at which small-scale waves are being refracted towards dissipative scales by interaction with larger-scale shear. Following *Gregg et al.* (2003), *Kunze et al.* (2006), and *Polzin et al.* (2013) the dissipation rate can be written as

$$\epsilon = \epsilon_0 \left(\frac{N}{N_0}\right)^2 \hat{E}^2 L(R_w, \theta) \qquad (2)$$

where $\hat{E}$ is a measure of the observed internal wave spectral level integrated out to k_c, R_w is the shear-to-strain ratio, which provides a measure of the average frequency content of a wavefield, and θ is latitude. $\hat{E}$ is typically calculated from vertical profiles of either shear or strain, which give estimates of kinetic and potential energy respectively. The $L(R_w, \theta)$ term includes the theoretical dependence on downscale energy transfer rate on both average wavefield frequency content (through R_w) and latitude (*Polzin et al.*, 1995; *Gregg et al.*, 2003).

In ideal circumstances both shear and strain are measured at vertical resolution comparable to the cutoff wavelength, approximately 10 meters. Realistically, many observations are limited in one way or another and a modified version of (2) is used. For example, the Lowered ADCP data used by *Kunze et al.* (2006) is noisy at scales smaller than about 50 m. They thus calculate $\hat{E}$ by integrating out measured spectra to the highest non-noisy wavenumber, typically much lower than the 'real' k_c would be, which can yield biased results. Other studies attempt to apply the method using measurements of either shear or strain alone, with an assumed valued of R_w (e.g. *Wijesekera et al.*, 1993), which can also bias results in regions where wave frequency varies.

In addition to measurement limitations, finescale parameterizations may be inappropriate where the underlying physics is not as assumed by theory. For example, the type of directly breaking internal tides observed by both *Klymak et al.* (2008) and *Alford et al.* (2011) require no spectral cascade and are not best described by a finescale model. Recent observations in the Southern Ocean also show a systematic elevation of finescale mixing estimates compared to those from a microstructure profiler (*Waterman et al.*, 2013a; *St. Laurent et al.*, 2012). *Waterman et al.* (2013b) suggest that wave-mean flow interactions may produce a different relationship between spectral variance levels and the rate of downscale energy transfer than predicted by the underlying theory. The method also fails in more subtle ways where downscale energy transfer is influenced by scattering from topography (*Kunze et al.*, 2002) or in shallow water (*MacKinnon and Gregg*, 2003).

Nevertheless, the method often produces values (Fig. 6) and patterns that are reasonable looking. Some examples of large-scale mixing patterns estimated using the finescale technique are shown in Figure 7 and discussed in Section 5.2. As the cottage industry of finescale measurements and methods continues to grow, further detailed comparison with microstructure measurements would provide useful groundtruthing.

5.2. Global values and patterns

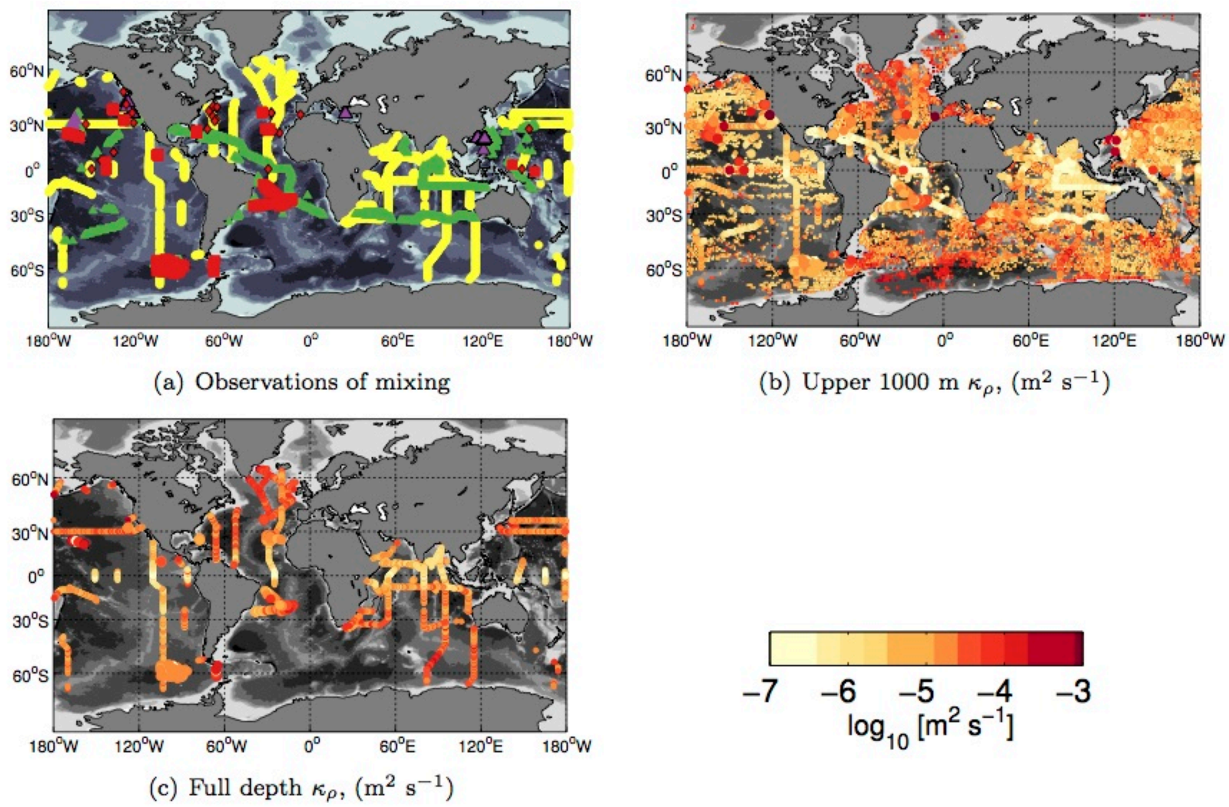

Figure 7: Reproduced from *Waterhouse et al.* (2013). a) Compiled observations of direct and indirect mixing measurements with red squares denoting microstructure measurements. Red ◇ are historical published microstructure measurements, green △ represent diffusivities calculated from ship board shear, yellow △ are inferred diffusivities from LADCP/CTD profiles of *Kunze et al.* (2006) and magenta △ are diffusivities calculated from overturns of density profiles from moored profilers. Depth averaged diffusivity, $\bar{\kappa}_\rho$, plotted as $\log_{10}$ [m^{2}s^{-1}] from b) the upper ocean (down to 1000 m) and c) from the full-water column. Background diffusivity map in b) comes from the strain based inferences of diffusivity of Whalen et al. [2012] from Argo floats.

The plethora of diapycnal mixing processes described above suggest a complex and evolving geography for mixing in the global ocean, of which microstructure observations sample an incredibly small portion. Most early microstructure measurements were limited to the upper ocean (*St. Laurent and Simmons*, 2006). Deep profiling, particularly to depths greater than 2000 m, did not become common practice until the 1990s (*Toole et al.*, 1994). *Waterhouse et al.* (2013) have compiled a significant percentage of available microstructure in the open ocean, the locations of which are shown in Figure 7a by red diamonds. Though the average microstructure-measured diffusivity below the main thermocline is on the order of 10^{-4} m^2 s^{-1} (*St. Laurent and Simmons*, 2006; *Waterhouse et al.*, 2013), estimates from different locations vary considerably reflecting the different dominant processes. Though the data is sparse, *Waterhouse et al.* (2013) compare available depth-integrated dissipation rates from microstructure to the global map of power input into the internal wave field and conclude that the sampling locations, taken as a set, are not especially biased towards energetic or quiet locations - in other words that the average observed 10^{-4} m^2 s^{-1} value is a reasonable one.

When mixing estimates from the finescale parameterization are included, a clearer pattern of mixing begins to emerge in both the upper (Fig. 7b) and deep ocean (Fig. 7c). Most of the data in the upper ocean comes from *Whalen et al.* (2012), who apply the finescale strain parameterization to 3 years of Argo profiles. They find strong correlations between elevated dissipation rates and topographic roughness (Sec. 4.1.1), mixed-layer inertial energy (Sec. 4.1.2) and mesoscale eddy kinetic energy (Sec. 4.3), and demonstrate a strong seasonal cycle to mixing in regions with energetic near-inertial motions (Sec. 3.2). Data is much sparser in the deep ocean, much of what's shown in Figure 7c comes from *Kunze et al.* (2006). They also find systematically elevated mixing above rough topography. Though the finescale parameterization comes with significant uncertainty and possibly systematic biases (Sec. 5.1), the coverage afforded provides geographical guidance for both future fieldwork planning and preliminary attempts to incorporate mixing patterns into large-scale models (Sec. 5.3).

5.3. Representing patchy mixing in large-scale models: progress and consequences

General circulation models used for climate research parameterize the impact of subgridscale processes, including turbulent mixing, because of their necessarily limited resolution. The current implementations generally do not include most of the spatial variability of mixing patterns described above (see *Simmons et al.* (2004a), *Jayne* (2009), and *Griffies et al.* (2010) for discussion of recent work). Below the surface mixed layer, climate models used in the IPCC-AR4 assessment (2007) employ a combination of a simple Richardson number parameterization for diffusivity and a horizontally uniform background diffusivity profile such as that suggested by *Bryan and Lewis* (1979) which crudely replicates the observed increase of diffusivity with depth. The Richardson-number dependent components (*Pacanowski and Philander*, 1981; *Large et al.*, 1994) are necessary for reasonable representation of large-scale shear flows such as the Equatorial Undercurrent, but rely on the resolved Richardson number to predict mixing. For almost all the processes described above, regional or global scale models will never be able to explicitly represent the motions with critical Richardson numbers. Often the limiting factor is horizontal rather than vertical resolution, as the nonlinear motions that directly lead to turbulence, such as breaking internal waves, have horizontal scales of kilometers or less.

Development of parameterizations that represent the full geography of diapycnal mixing are essential, as evidence is accumulating that patchy mixing can have significant consequences for global circulation patterns. Since both the magnitude and distribution of diapycnal mixing are likely to change in a future climate (as, for example, wind stress patterns evolve), accurate prediction of future or past climate requires development of parameterizations of turbulent mixing that are based on appropriate physics. In the last decade a spate of studies have shown that many features of global ocean circulation are sensitive to the distribution of diapycnal mixing, thorough reviews of which can be found in *Jayne* (2009) and *Friedrich et al.* (2011).

The US Climate Variability and Predictability (CLIVAR) Program recently established a series of Climate Process Teams (CPTs) to develop and implement parameterizations for unresolved processes in climate models. One of these CPTs focused on mixing and entrainment in overflows, with results described in *Legg et al.* (2009) and *Danabasoglu et al.* (2010). A combination of data analysis, theory and idealized numerical modeling led to, among other things, the development of an improved formulation for mixing related to shear instability that allowed for vertical transport of turbulence over a larger region than just that of unstable local Richardson number (*Jackson et al.*, 2008). Implementation of this new scheme in global models improved representations of both deep overflows and other strongly sheared flows like the Pacific Equatorial Undercurrent (*Legg et al.*, 2009).

The first substantial attempt to parameterize internal-wave driven mixing was to represent the nearfield part of internal tide dissipation, that is the portion of generated internal waves that break near rough topography at which they are created. The result is a global map of dissipation that mirrors that of internal tide generation spots, with most of the elevated mixing at depth (*St. Laurent et al.*, 2002). The parameterization is essentially given by the product of power going into internal tides, itself a function of topographic roughness, barotropic tidal strength and deep stratification, and an empirically derived vertical decay scale to represent the observed enhancement of turbulent mixing at depth. This scheme is now implemented in the Community Climate System Model (CCSM4) of NCAR (*Jayne*, 2009; *Gent*

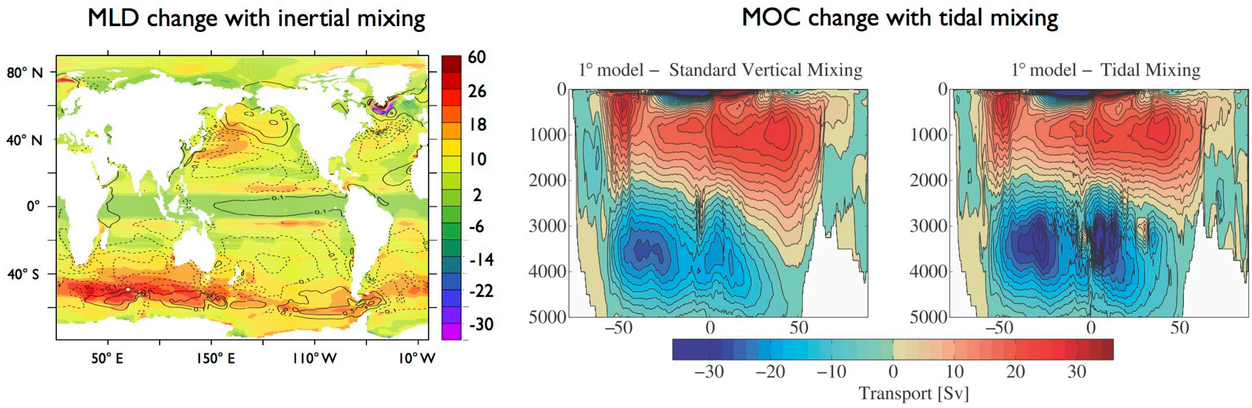

Figure 8: Examples of the sensitivity of large-scale circulation patterns to diapyncal mixing parametereizations in the upper and deep ocean. Left: change in mixed-layer depths, in meters, when near-inertial motions are explicitly represented in a global model, reproduced from *Jochum et al.* (2013). Right: snapshots of the modeled MOC using a standard parameterization for diapycnal diffusivity and one that includes elevated mixing over rough topography, reproduced from *Jayne* (2009).

et al., 2011), the Modular Ocean Model of GFDL (*Simmons et al.*, 2004a) and GFDL's Generalized Ocean Layer Dynamics model (GOLD). The parameterization appears to significantly modify circulation patterns, particularly by enhancing the deep limb of the MOC (Fig. 8 and *Jayne* (2009)). An updated version with a vertical structure function based on wave-wave interaction dynamics as described in *Polzin* (2009) is now being tested at GFDL with promising results (*Melet et al.*, 2013).

More generally, heterogeneous diapycnal fluxes in the abyssal ocean rule out the Stommel-Arons conceptual picture, in which deep diapycnal upwelling stretches water columns and leads to uniform poleward flow to conserve potential vorticity (*Stommel and Arons*, 1960). Instead, isolated mixing hotspots should lead to limited regions of meridional flow (*Samelson*, 1998; *Huang and Jin*, 2002; *Katsman*, 2006; *Emile-Geay and Madec*, 2009), as indicated in observations (*Davis*, 1998; *Hogg and Owens*, 1999; *St.Laurent et al.*, 2001). Furthermore, certain profiles of bottom-enhanced turbulent buoyancy fluxes can actually lead to local diapycnal downwelling, with consequent substantial changes in the abyssal circulation (*Simmons et al.*, 2004a; *Saenko and Merryfield*, 2005) . A variety of recent modeling studies show that everything from the strength of the MOC to the deep ocean stratification to the distribution of passive tracers respond to changing patterns of imposed deep diffusivity (*Hasumi and Suginohara*, 1999; *Scott and Marotzke*, 2002; *Simmons et al.*, 2004a; *Gnanadesikan et al.*, 2004; *Saenko and Merryfield*, 2005; *Palmer et al.*, 2007; *Friedrich et al.*, 2011). Though the nature of the circulation changes is not entirely consistent between models, the sensitivity to mixing patterns is a persistent feature of such experiments, making an improved understanding and parameterization of the processes described in this chapter essential.

The geography of upper ocean mixing also has significant impact on circulation, water properties, fluxes of heat, dissolved greenhouse gasses and biologically essential nutrients (*Harrison and Hallberg*, 2008). For example, an initial stab at representing mixing in the upper ocean from near-inertial motions is described by *Jochum et al.* (2013). Their first step was to increase the frequency of ocean-atmosphere coupling to every two hours, which allowed generation of an energetic field of near-inertial motions in the mixed layer. Their second step was to parameterize mixing due to unresolved vertically propagating near-inertial internal waves using an ad-hoc vertical decay scale. The results suggest that NIWs lead to a 20-50% deeper ocean mixed layer under the storm tracks and the trade winds, largely from inertial shear at the mixed-layer base (Fig. 8b). Of particular note, the tropical deepening leads to a cooler SST and a substantial shift in global precipitation, sea level pressure and the resulting surface winds. Upper ocean mixing is also crucial for supplying nutrients to the euphotic zone, and changes in the rate and pattern of diapycnal nutrient fluxes may have significant effects on primary production rates (*Gnanadesikan et al.*, 2002).

While these attempts are a good start, only a fraction of the internal wave energy available for mixing is represented. So far, unaccounted for are about 2/3 of a TW in the low mode internal tides, most of the power in near inertial internal waves, high-frequency breaking waves in the upper ocean, and lee waves in the Southern Ocean. Attempts are underway as part of a new CPT to develop and refine related parameterizations for diapycnal mixing related to internal-wave breaking. However for many of the mixing processes described in this chapter the relevant physics is not yet well enough understood.

6. Summary and future directions

The search for observations confirming the expected levels of mixing in the ocean interior has revealed enormous geographical variability and an incredibly rich range of turbulent processes. Overall there appears to be approximately the same power available to turbulent mixing as is required to drive the deep overturning circulation. Over the last decade, emphasis has moved towards an appreciation of the complex patterns of mixing in space and time and the diverse range of associated dynamics. The next step is to tease apart how the specific geography of mixing (Fig. 7) is compatible with the details of water mass transformation in individual basins. For example, *Huussen et al.* (2012) look at the energy budget for the Indian Ocean equatorward of 32S. They find that while there is overall consistency between the power available in the internal wave field and that required for water mass transformation by inverse models, there is a discrepancy in depths. In particular, they find that mixing at mid-depths inferred by a finescale parameterization (1000-3000 m) is not sufficient to produce the required water mass transformations. Further efforts to approach such problems from all angles are clearly needed. Though there is no shortage of pressing open questions, we find the following one particularly intriguing:

- Where does the low-mode internal wave energy seen crossing ocean basins dissipate? What percentage of the energy dissipates steadily as waves propagate and what percent dissipates when waves hit continental slopes? If the latter is large, what are the implications for regional and basin-wide circulation patterns?

- What percentage of mesoscale energy is dissipated through irreversible mixing in the stratified ocean interior? What are the dominant processes? Is the dissipation primarily in the deep or upper ocean?

- What is the role of strong, often hydraulically controlled mixing near fracture zones or other deep rough topography? Can the resultant mixed fluid be exported to form a significant percentage of diapycnal mass transport across certain isopycnals?

Moving into the next decade, we expect that new observations will continue to be a primary driver of progress. Microstructure sensors are moving beyond the traditional vertical profilers onto a range of platforms, including fixed-point moorings (*Moum and Nash*, 2009), autonomous underwater vehicles (AUVs) and gliders (*Wolk et al.*, 2009), horizontally towed vehicles, and even onto the CTD rosette (J. Nash, pers. comm.). In situations where dissipation rates are set by the rate of energy cascade from large to small scales, mixing may be inferred from finescale measurements of the internal wave field, or direct measurements of the outer scales of turbulent overturns (Secs. 2,5.1), both of which can be made by a growing variety of ship-based and autonomous instruments such as Argo floats. Finally, increasingly high-resolution models are proving invaluable for looking at everything from the details of turbulent instabilities at the smallest scales (*Venayagamoorthy and Fringer*, 2012; *Smyth and Moum*, 2012), to global patterns of internal wave propagation and destruction (*Simmons*, 2008; *Arbic et al.*, 2012). We have every expectation that the next decade of ocean mixing research will bring new surprises.

Acknowledgments

We are very appreciative for the detailed and thoughtful comments of 9 reviewers, which have considerably improved the perspective and precision of the text. JAM and LStL are participants in an NSF and NOAA funded Climate Process Team, within with many relevant discussions have occurred.

References

Alford, M., and M. Gregg (2001), Near-intertial mixing: Modulation of shear, strain and microstructure at low latitude, *J. Geophys. Res.*, *106*(C8), 16,947–16,968.

Alford, M., and R. Pinkel (2000), Observations of overturning in the thermocline: The context of ocean mixing, *J. Phys. Oceanogr.*, *30*(5), 805–832.

Alford, M. H. (2001), Internal swell generation: The spatial distribution of energy flux from the wind to mixed layer near-inertial motions, *J. Phys. Oceanogr.*, *31*, 2359–2368.

Alford, M. H. (2003), Energy available for ocean mixing redistributed though long-range propagation of internal waves, *Nature*, *423*, 159–163.

Alford, M. H. (2008), Observations of parametric subharmonic instability of the diurnal internal tide in the South China Sea, *Geophys. Res. Lett.*, *35*(L15602), doi: 10.1029/2008GLO34,720.

Alford, M. H. (2010), Sustained, full-water-column observations of internal waves and mixing near Mendocino Escarpment, *J. Phys. Oceanogr.*, *40*, 2643–2660.

Alford, M. H., and M. Whitmont (2007), Seasonal and spatial variability of near-inertial kinetic energy from historical moored velocity records, *J. Phys. Oceanogr.*, *37*(8), 2022–2037.

Alford, M. H., J. A. MacKinnon, Z. Zhao, R. Pinkel, J. Klymak, and T. Peacock (2007), Internal waves across the Pacific, *Geophys. Res. Lett*, *34*(doi:10.1029/2007GL031566).

Alford, M. H., et al. (2011), Energy flux and dissipation in Luzon Strait: two tales of two ridges, *J. Phys. Oceanogr.*, *41*(11), 2211–2222.

Alford, M. H., M. F. Cronin, and J. M. Klymak (2012), Annual cycle and depth penetration of wind-generated near-inertial internal waves at Ocean Station Papa in the Northeast Pacific, *J. Phys. Oceanogr.*, *42*(6), 889–909.

Althaus, A., E. Kunze, and T. Sanford (2003), Internal tide radiation from Mendocino Escarpment, *J. Phys. Oceanogr.*, *33*, 1510–1527.

Arbic, B. K., J. G. Richman, J. F. Shriver, P. G. Timko, E. J. Metzger, and A. J. Wallcraft (2012), Global Modeling of Internal Tides Within an Eddying Ocean General Circulation Model, *Oceanography*, *25*(2), 20–29.

Belcher, S. E., et al. (2012), A global perspective on mixing in the ocean surface boundary layer, *Geophys. Res. Lett.*, *39*(18), doi: 10.1029/2012GL052932.

Boccaletti, G., R. Ferrari, and B. Fox-Kemper (2007), Mixed layer instabilities and restratification, *Journal of Physical Oceanography*, *37*(9), 2228–2250.

Bryan, K., and L. Lewis (1979), A water mass model of the world ocean, *J. Geophys. Res.*, *84*, 2503–2517.

Bryden, H. L., and A. J. G. Nurser (2003), Effects of strait mixing on ocean stratification, *J. Phys. Oceanogr.*, *33*(8), 1870–1872.

Buhler, O., and M. McIntyre (2005), Wave capture and wave-vortex duality, *J. Fluid Mech.*, *534*, 67–95.

Capet, X., J. C. McWilliams, M. J. Molemaker, and A. F. Shchepetkin (2008), Mesoscale to submesoscale transition in the California Current System. part ii: Frontal processes, *J. Phys. Oceanogr.*, *38*(1), 44–64.

Carter, G. S., and M. C. Gregg (2006), Persistent near-diurnal internal waves observed above a site of M_2 barotropic-to-baroclinic conversion, *J. Phys. Oceanogr.*, *36*(6), 1136–1147.

Chaigneau, A., O. Pizarro, and W. Rojas (2008), Global climatology of near-inertial current characteristics from Lagrangian observations, *Geophys. Res. Lett*, *35*, L13,603, doi:10.1029/2008GL034060, doi:10.1029/2008GL034060.

Cole, S. T., D. L. Rudnick, and B. A. Hodges (2009), Observations of tidal internal wave beams at Kauai Channel, Hawaii, *J. Phys. Oceanogr.*, *39*, 421–436.

Craik, A., and S. Leibovich (1976), A rational model for Langmuir circulations, *J. Fluid Mech.*, *73*, 401–426.

Crawford, G. B., and W. G. Large (1996), A numerical investigation of resonant inertial response of the ocean to wind forcing, *J. Phys. Oceanogr.*, *26*, 873–891.

Danabasoglu, G., W. G. Large, and B. B. Briegleb (2010), Climate impacts of parameterized Nordic Sea overflows, *J. Geophys. Res.*, *115*, doi:10.1029/2010JC006,243.

Danioux, E., P. Klein, and P. Riviere (2008), Propagation of wind energy into the deep ocean through a fully turbulent mesoscale eddy field, *J. Phys. Oceanogr.*, *38*, 2224–2241.

D'Asaro, E. (1985), The energy flux from the wind to near-inertial motions in the mixed layer, *J. Phys. Oceanogr.*, *15*, 943–959.

D'Asaro, E., C. Eriksen, M. Levine, P. Niller, C. Paulson, and P. van Meurs (1995), Upper-ocean inertial currents forced by a strong storm. Part 1: Data and comparisons with linear theory, *J. Phys. Oceanogr.*, *25*, 2909–2936.

D'Asaro, E. A., and R.-C. Lien (2000), The wave-turbulence transition for stratified flows, *J. Phys. Oceanogr.*, *30*(7), 1669–1678.

D'Asaro, E. A., C. Lee, L. Rainville, R. Harcourt, and L. Thomas (2011), Enhanced turbulence and energy dissiaption at ocean fronts, *Science*, *332*, 318–322.

Davis, R. E. (1998), Preliminary results from directly measuring mid-depth circulation in the tropical and South Pacific, *J. Geophys. Res.*, *103*, 24,619–39.

Dewar, W., R. Bingham, and R. Iverson (2006), Does the marine biosphere mix the ocean?, *J. Mar. Res.*, *64*(4), 541–561.

Dewar, W. K., and A. M. Hogg (2010), Topographic inviscid dissipation of balanced flow, *Ocean Modelling*, *32*, 1–13.

Dillon, T. M. (1982), Vertical overturns: A comparison of Thorpe and Ozmidov length scales, *J. Geophys. Res.*, *87*, 9601–9613.

Donohue, K., and J. Toole (2003), A near-synoptic survey of the Southwest Indian Ocean, *Deep-Sea Res II*, *50*, 1893–1931.

Egbert, G. D., and R. D. Ray (2001), Estimates of M2 tidal energy dissipation from TOPEX/Poseidon altimeter data, *J. Geophys. Res.*, *106*(C10), 22,475–22,502.

Elipot, S., R. Lumpkin, and G. Prieto (2010), Intertial oscillations modification by mesoscale vorticity, *J. Geophys. Res.*, *114*(C06003), doi:10.1029/2008JC005,170.

Emile-Geay, J., and C. Madec (2009), Geothermal heating, diapycnal mixing and the geothermal heating, diapycnal mixing and the abyssal circulation, *Ocean Sci.*, *5*, 203–217.

Eriksen, C. (1998), Internal wave reflection and mixing at Fieberling Guyot, *J. Geophys. Res.*, *103*, 2977–94.

Eriksen, C. C. (1985), Implications of ocean bottom reflection for internal wave spectra and mixing, *J. Phys. Oceanogr.*, *15*, 1145–1156.

Ferrari, R., and C. Wunsch (2009), Ocean circulation kinetic energy: reservoirs, sources, and sinks, *Ann. Rev. Fluid Mech.*, *41*, 253–82.

Ferrari, R., J. McWilliams, V. Canuto, and M. Dubovikov (2008), Parameterization of eddy fluxes near oceanic boundaries, *Journal of Climate*, *21*, 2770–2789.

Ferrari, R., S. M. Griffies, A. Nurser, and G. Vallis (2010), A boundary-value problem for the parameterized mesoscale eddy transport, *Ocean Modelling*, *32*, 143–156.

Ferron, B., H. Mercier, K. Speer, A. Gargett, and K. Polzin (1998), Mixing in the Romanche Fracture Zone, *J. Phys. Oceanogr.*, *28*(10), 1929–1945.

Forryan, A., A. C. N. Garabato, K. L. Polzin, and S. N. Waterman (2013), Rapid injection of near-inertial kinetic energy into the stratified upper ocean at an Antarctic Circumpolar Current front, *J. Geophys. Res. Oceans*, *submitted*.

Fox-Kemper, B., R. Ferrari, and R. Hallberg (2008), Parameterization of mixed layer eddies. part i: Theory and diagnosis, *J. Phys. Oceanogr.*, *38*(6), 1145–1165.

Friedrich, T., A. Timmermann, T. Decloedt, D. Luther, and A. Mouchet (2011), The effect of topography-enhanced diapycnal mixing on ocean and atmospheric circulation and marine biogeochemistry, *Ocean Modelling*, *39*, 262–274.

Furuichi, N., T. Hibiya, and Y. Niwa (2005), Bispectral analysis of energy transfer within the two-dimensional oceanic internal wave field, *Journal of Physical Oceanography*, *35*, 2104–2109.

Ganachaud, A., and C. Wunsch (2000), Improved estimates of global ocean circulation, heat transport and mixing from hydrographic data, *Nature*, *408*, 453–457.

Gargett, A. E. (1990), Do we really know how to scale the turbulent kinetic energy dissipation rate ϵ due to breaking of oceanic internal waves?, *J. Geophys. Res.*, *95*(C9), 15,971–15,974.

Garrett, C. (1991), Marginal mixing theories, *Atmosphere-Ocean*, *29*(2), 313–339.

Garrett, C. (2001), An isopycnal view of near-boundary mixing and associated flows, *J. Phys. Oceanogr.*, *31*(1), 138–142.

Garrett, C., and E. Kunze (2007), Internal tide generation in the deep ocean, *Ann. Rev. of Fluid Mech.*, *39*, 57–87, doi: 10.1146/annurev.fluid.39.050,905.110,227.

Gent, P. R., et al. (2011), The community climate system model version 4, *J. Climate*, *24*(19), 4973–4991.

Gerkema, T., C. Staquet, and P. Bouruet-Aubertot (2006), Non-linear effects in internal-tide beams, and mixing, *Ocean Modelling*, *12*(3-4), 302–318.

Gilbert, D., and C. Garrett (1989), Implications for ocean mixing of internal wave scattering off irregular topography, *J. Phys. Oceanogr.*, *19*(11), 1716–1729.

Gill, A. (1984), On the behavior of internal waves in the wakes of storms, *J. Phys. Oceanogr.*, *14*(7), 1129–1151.

Gill, A. E. (1982), *Atmosphere-Ocean Dynamics*, 662 pp., Academic.

Gnanadesikan, A., R. Slater, N. Gruber, and J. Sarmiento (2002), Oceanic vertical exchange and new production: a comparison between models and observations, *Deep-Sea Res II*, *49*(1-3), 363–401.

Gnanadesikan, A., J. Dunne, R. Key, K. Matsumoto, J. Sarmiento, and R. Slater (2004), Oceanic ventilation and biogeochemical cycling: understanding the physical mechanisms that produce realistic distributions of tracers and productivity., *Global Biogeochem. Cycles*, *18*(4), GB4010.

Grant, A. L., and S. E. Belcher (2009), Characteristics of Langmuir turbulence in the ocean mixed layer, *J. Phys. Oceanogr.*, *39*(8), 1871–1887.

Gregg, M. (1987), Diapycnal mixing in the thermocline, *J. Geophys. Res.*, *92*(C5), 5249–5286.

Gregg, M. (1998), Estimation and geography of diapycnal mixing in the stratified ocean, in *Physical processes in lakes and oceans*, edited by J. Imberger, Coastal and Estuarine Studies, pp. 305–338, American Geophysical Union.

Gregg, M., H. Peters, J. Wesson, N. S. Oakey, and T. Shay (1985), Intensive measurements of turbulence and shear in the equatorial undercurent, *Nature*, *318*(140-144).

Gregg, M. C. (1989), Scaling turbulent dissipation in the thermocline, *J. Geophys. Res.*, *94*(C7), 9686–9698.

Gregg, M. C., and E. Kunze (1991), Shear and strain in Santa Monica Basin, *J. Geophys. Res.*, *96*(C9), 16,709–16,719.

Gregg, M. C., T. B. Sanford, and D. P. Winkel (2003), Reduced mixing from the breaking of internal waves in equatorial waters, *Nature*, *422*, 513–515.

Gregg, M. C., R. A. Hall, G. S. Carter, M. H. Alford, R. Lien, D. P. Winkel, and D. J. Wain (2011), Flow and mixing in Ascension, a steep, narrow canyon, *J. Geophys. Res.*, *116*(C07016), doi:doi:10.1029/2010JC006610.

Griffies, S., et al. (2010), Problems and prospects in large-scale ocean circulation models, in *Proceedings of OceanObs'09: Sustained Ocean Observations and Information for Society, , Venice, Italy, 21-25 September 2009*, vol. 2, edited by J. Hall, D. Harrison, and D. Stammer, ESA Publication WPP-306, doi:doi:10.5270/OceanObs09.cwp.38.

Haine, T. W. N., and J. Marshall (1998), Gravitational, symmetric, and baroclinic instability of the ocean mixed layer, *J. Phys. Oceanogr.*, *28*, 634–658.

Harrison, M., and R. Hallberg (2008), Pacific subtropical cell response to reduced equatorial dissipation, *J. Phys. Oceanogr.*, *38*(9), 1894–1912.

Hasumi, H., and N. Suginohara (1999), Effects of locally enhanced vertical diffusivity over rough bathymetry on the world ocean circulation, *J. Geophys. Res.*, *104*, 23,367–23,374.

Hazewinkel, J., and K. Winters (2011), Psi of the internal tide on a -plane: Flux divergence and near-inertial wave propagation, *J. Phys. Oceanogr.*, *41*(9), 1673–1682.

Henyey, F. S., J. Wright, and S. M. Flatté (1986), Energy and action flow through the internal wave field, *J. Geophys. Res.*, *91*, 8487–8495.

Heywood, K., A. Naveira Garabato, and D. Stevens (2002), High mixing rates in the abyssal Southernn Ocean, *Nature*, *415*, 1011–1013.

Hibiya, T., and M. Nagasawa (2004), Latitudinal dependence of diapycnal diffusivity in the thermocline estimated using a finescale parameterization, *Geophysical Research Letters*, *31*(LO1301).

Hibiya, T., M. Nagasawa, and Y. Niwa (2002), Nonlinear energy transfer within the oceanic internal wave spectrum at mid and high latitudes, *J. Geophys. Res.*, *107*(C11).

Hogg, N. G., and W. B. Owens (1999), Direct measurements of hte deep circulation with the Brazil Basin, *Deep-Sea Research II*, *46*, 335–353.

Hosegood, P., M. C. Gregg, and M. H. Alford (2006), Sub-mesoscale lateral density structure in the oceanic surface mixed layer, *Geophys. Res. Lett.*, *33*(22), DOI: 10.1029/2006GL026,797.

Huang, R., and X. Jin (2002), Deep circulation in the South Atlantic induced by bottom-intensified mixing over the midocean ridge, *J. Phys. Oceanogr.*, *32*, 1150–1164.

Huang, R. X. (1998), On the balance of energy in the oceanic general circulation, *Scientia Atmospherica Sinica*, *4*.

Hughes, G. O., A. M. C. Hogg, and R. W. Griffiths (2009), Available potential energy and irreversible mixing in the meridional overturning circulation, *Journal of Physical Oceanography*, *39*(12), 3130–3146.

Huussen, T. N., A. C. Naveira-Garabato, H. L. Bryden, and E. L. McDonagh (2012), Is the deep Indian Ocean MOC sustained by breaking internal waves?, *J. Geophys. Res.*, *117*(C8), C08,024.

Ivey, G., K. Winters, and J. Koseff (2008), Density stratification, turbulence, but how much mixing?, *Ann. Rev. Fluid Mech.*, *40*, 169–184.

Ivey, G. N., K. B. Winters, and I. P. D. DeSilva (2000), Turbulent mixing in a sloping benthic boundary layer energized by internal waves, *J. Fluid Mech.*, *418*, 59–76.

Jackson, L., R. Hallberg, and S. Legg (2008), A parameterization of shear-driven turbulence for ocean climate models, *J. Phys. Oceanogr.*, *38*(5), 1033–1053.

Jayne, S., and L. C. St. Laurent (2001), Parameterizing tidal dissipation over rough topography, *Geophys. Res. Lett.*, *28*, 811–814.

Jayne, S. R. (2009), The impact of abyssal mixing parameterizations in an ocean general circulation model, *J. Phys. Oceanogr.*, *39*, 1756–1775.

Jiang, J., Y. Lu, and W. Perrie (2005), Estimating the energy flux from the wind to ocean inertial motions: The sensitivity to surface wind fields, *Geophys. Res. Lett.*, *32*(L15610), doi:10.1029/2005GL023,289.

Jing, Z., and L. Wu (2010), Seasonal variation of turbulent diapycnal mixing in the northwestern Pacific stirred by wind stress, *Geophys. Res. Lett.*, *37*(doi:10.1029/2010GL045418).

Jochum, M., B. P. Briegleb, G. Danabasoglu, W. G. Large, N. J. Norton, S. R. Jayne, M. H. Alford, and F. O. Bryan (2013), The impact of oceanic near-inertial waves on climate., *J. Climate*, *in press*, doi:10.1175/JCLI-D-12-00181.1.

Johnston, T. M. S., and D. L. Rudnick (2009), Observations of the transition layer, *J. Phys. Oceanogr.*, *39*, 780–797.

Johnston, T. M. S., M. A. Merrifield, and P. E. Holloway (2003), Internal tide scattering at the Line Islands Ridge, *J. Geophys. Res.*, *108*, 3365, doi:10.1029/2003JC001844.

Johnston, T. S., D. L. Rudnick, and G. S. Carter (2011), Internal tidal beams and mixing near Monterey Bay, *J. Geophys. Res.*, *116*(10.1029/2010JC006592).

Katsman, C. A. (2006), Impacts of localized mixing and topography on the stationary abyssal circulation, *J. Phys. Oceanogr.*, *36*, 1660–1671.

Kelly, S., J. Nash, K. Martini, M. Alford, and E. Kunze (2011), Internal-tide generation and scattering on a continental slope, *J. Phys. Oceanogr*, *in press*.

Kelly, S. M., and J. D. Nash (2010), Internal-tide generation and destruction by shoaling internal tides, *Geophys. Res. Lett.*, *37*(23).

Klocker, A., and T. McDougall (2010), Influence of the nonlinear equation of state on global estimates of dianeutral advection and diffusion, *J. Phys. Oceanogr.*, *40*(8), 1690–1709.

Klymak, J. M., J. N. Moum, J. D. Nash, E. Kunze, J. B. Girton, G. S. Carter, C. M. Lee, T. B. Sanford, and M. C. Gregg (2006), An estimate of tidal energy lost to turbulence at the Hawaiian Ridge, *J. Phys. Oceanogr.*, *36*, 1148–1164.

Klymak, J. M., R. Pinkel, and L. Rainville (2008), Direct breaking of the internal tide near topography: Kaena Ridge, Hawaii, *J. Phys. Oceanogr.*, *38*, 380–399.

Klymak, J. M., S. Legg, and R. Pinkel (2010a), A simple parameterization of turbulent tidal mixing near supercritical topography, *J. Phys. Oceanogr.*, *40*(9), 2059–2074.

Klymak, J. M., M. H. Alford, R. Pinkel, R. C. Lien, and Y. J. Yang (2010b), The breaking and scattering of the internal tide on a continental slope, *J. Phys. Ocean.*, *in press*, doi:10.1175/2010JPO4500.1.

Klymak, J. M., S. Legg, M. H. Alford, M. Buijsman, R. Pinkel, and J. D. Nash (2012), The Direct Breaking of Internal Waves at Steep Topography, *Oceanography*, *25*(2), 150–159.

Kuhlbrodt, T., A. Griesel, M. Montoya, A. Levermann, M. Hofmann, and S. Rahmstorf (2007), On the driving processes of the Atlantic Meridional Overturning Circulation, *Rev. Geophys*, *45*, doi:10.1029/2004RG000,166.

Kunze, E. (1985), Near-inertial wave propagation in geostrophic shear, *J. Phys. Oceanogr.*, *15*(5), 544–565.

Kunze, E., R. W. Schmitt, and J. M. Toole (1995), The energy balance in a warm-core ring's near-inertial critical layer, *J. Phys. Oceanogr.*, *25*, 942–957.

Kunze, E., L. K. Rosenfeld, G. S. Carter, and M. C. Gregg (2002), Internal waves in monterey submarine canyon, *J. Phys. Oceanogr.*, *32*(6), 1890–1913.

Kunze, E., E. Firing, J. M. Hummon, T. K. Chereskin, and A. M. Thurnherr (2006), Global abyssal mixing inferred from lowered ADCP shear and CTD strain profiles, *J. Phys. Oceanogr.*, *36*(8), 1553–1576.

Kunze, E., C. MacKay, E. E. McPhee-Shaw, K. Morrice, J. B. Girton, and S. R. Terker (2012), Turbulent Mixing and Exchange with Interior Waters on Sloping Boundaries, *J. Phys. Oceanogr.*, *42*(6), 910–927, doi:10.1175/JPO-D-11-075.1.

Lapeyre, G., P. Klein, and B. L. Hua (2006), Oceanic restratification forced by surface frontogenesis, *J. Phys. Oceanogr.*, *36*(8), 1577–1590.

Large, W., J. McWilliams, and S. Doney (1994), Oceanic vertical mixing - a review and a model with a nonlocal boundary-layer paramaterization, *Reviews of Geophysics*, *32*(4), 363–403.

Large, W. G., and A. J. G. Nurser (2001), Ocean surface water mass transformation, in *Ocean Circulation and Climate*, *International Geophysics Series*, vol. 77, edited by G. Seidler, J. Church, and J. Gould, Academic Press.

Ledwell, J., A. Watson, and C. Law (1993), Evidence for slow mixing across the pycnocline from an open-ocean tracer-release experiment, *Nature*, *364*, 701–703.

Ledwell, J., E. Montgomery, K. Polzin, L. St Laurent, R. Schmitt, and J. Toole (2000), Evidence for enhanced mixing over rough topography in the abyssal ocean, *Nature*, *403*(6766), 179–182.

Ledwell, J. R., A. J. Watson, and C. S. Law (1998), Mixing of a tracer in the pycnocline, *J. Geophys. Res.*, *103*(C10), 21,499–21.

Ledwell, J. R., L. C. St. Laurent, J. B. Girton, and J. M. Toole (2011), Diapycnal mixing in the Antarctic Circumpolar Current, *J. Phys. Oceanogr.*, *41*, 241–246.

Legg, S. (2012), Overflows and convectively driven flows, in *Buoyancy-Driven Flows*, edited by E. Chassignet, C. Cenedese, and J. Verron, pp. 203–239, Cambridge Univ. Press.

Legg, S., and J. M. Klymak (2008), Internal hydrualic jumps and overturning generated by tidal flow over a steep ridge, *J. Phys. Oceanogr.*, pp.

1949–1964.
Legg, S., et al. (2009), Improving oceanic overflow representation in climate models: the gravity current entrainment climate process team, *Bulletin of the American Meteorological Society*, *90*(5).
Li, M., C. Garrett, and E. Skyllingstad (2005), A regime diagram for classifying turbulence large eddies in the upper ocean, *Deep Sea Research Part I: Oceanographic Research Papers*, *52*(2), 259–278.
Lien, R.-C., and M. Gregg (2001), Observations of turbulence in a tidal beam and across a coastal ridge, *J. Geophys. Res.*, *106*, 4575–4591.
Lien, R.-C., E. A. D'Asaro, and M. McPhaden (2002), Internal waves and turbulence in the Upper Centeral Equatorial Pacific: Lagrangian and eulerian observations, *J. Phys. Oceanogr.*, *32*(9), 2619–2639.
Lueck, R., F. Wolk, and H. Yamazaki (2002), Oceanic velocity microstructure measurements in the 20th century, *Journal of oceanography*, *58*(1), 153–174.
Lueck, R. G., and T. D. Mudge (1997), Topographically induced mixing around a shallow seamount, *Science*, *276*, 1831–1833.
Lumpkin, R., and K. Speer (2007), Global Ocean Meridional Overturning, *J. Phys. Oceanogr.*, *37*, 2550–2562.
Lvov, Y. V., K. L. Polzin, and E. G. Tabak (2004), Energy spectra of the ocean's internal wave field: Theory and observations, *Physical Review Letters*, *92*(12), 128,501–1–4.
Lvov, Y. V., K. L. Polzin, E. G. Tabak, and N. Yokoyama (2010), Oceanic internal wavefield: theory of scale-invariant spectra, *J. Phys. Oceanogr.*, *40*, 2605–2623.
MacKinnon, J., and M. Gregg (2003), Mixing on the late-summer New England shelf – solibores, shear and stratification, *JPO*, *33*(7), 1476–1492.
MacKinnon, J. A., and K. Winters (2005), Subtropical catastrophe: significant loss of low-mode tidal energy at 28.9 degrees, *Geophysical Research Letters*, *32*(15), doi:10.1029/2005GL023,376.
MacKinnon, J. A., and K. B. Winters (2003), Spectral evolution of bottom-forced internal waves, in *Near-Boundary Processes and Their Parameterization, Proceedings of the 13th 'Aha Huliko'a Hawaiian Winter Workshop*, edited by P. Muller and D. Henderson, pp. 73–83.
MacKinnon, J. A., T. M. S. Johnston, and R. Pinkel (2008), Strong transport and mixing of deep water through the Southwest Indian Ridge, *Nature Geosciences*, *1*, 755–758.
MacKinnon, J. A., M. H. Alford, O. Sun, R. Pinkel, Z. Zhao, and J. Klymak (2013), Parametric subharmonic instability of the internal tide at 29N, *J. Phys. Ocean.*, *43*(1), 17–28.
Mahadevan, A., A. Tandon, and R. Ferrari (2010), Rapid changes in mixed layer stratification driven by submesoscale instabilities and winds, *J. Geophys. Res.*, *115*, doi:10.1029/2008JC005,203.
Marshall, J., and T. Radko (2006), A model of the upper branch of the meridional overturning of the Southern Ocean, *Prog. Oceanogr.*, *70*, 331–345.
Martin, J. P., D. L. Rudnick, and R. Pinkel (2006), Spatially broad observations of internal waves in the upper ocean at the hawaiian ridge, *J. Phys. Ocean.*, *36*(6), 1085–1103.
Martini, K. I., M. H. Alford, E. Kunze, S. H. Kelly, and J. D. Nash (2011), Observations of internal tides on the Oregon continental slope, *J. Phys. Oceanogr.*, *41*(9), 1772–1794.
McComas, C. H., and P. Müller (1981), The dynamic balance of internal waves, *J. Phys. Oceanogr.*, *11*, 970–986.
McPhee-Shaw, E., and E. Kunze (2002), Boundary layer intrusions from a sloping bottom: A mechanism for generating intermediate nepheloid layers, *J. Geophys. Res. Oceans*, *107*(C6), doi:10.1029/2001JC000801.
McWilliams, J., P. Sullivan, and C. Moeng (1997), Langmuir turbulence in the ocean, *J. Fluid Mech.*, *334*, 1–30.
McWilliams, J., J. Restrepo, and E. Lane (2004), An asymptotic theory for the interaction of waves and currents in coastal waters, *Journal of Fluid Mechanics*, *511*, 135–178.
Melet, A., R. Hallberg, S. Legg, and K. Polzin (2013), Sensitivity of the Pacific Ocean state to the vertical distribution of internal-tide driven mixing, *J. Phys. Oceanogr.*, *In press*, doi:10.1175/JPO-D-12-055.1.
Mihaly, S. F., R. Thomson, and A. B. Rabinovich (1998), Evidence for nonlinear interaction between internal waves of inertial and semidiurnal frequency, *Geophys. Res. Lett.*, *25*(8), 1205–1208.
Moehlis, J., and S. G. Llewellyn-Smith (2001), Radiation of mixed layer near-inertial oscillations into the ocean interior, *J. Phys. Oceanogr.*, *31*, 1550–1560.
Molemaker, M. J., J. C. McWilliams, and I. Yavhen (2005), Baroclinic instability and loss of balance, *J. Phys. Oceanogr.*, *35*(9), 1505–1517.
Moum, J., and W. Smyth (2001), *Encyclopedia of Ocean Sciences*, chap. Upper ocean mixing, pp. 3093–3100, Academic Press.
Moum, J., M. C. Gregg, R.-C. Lien, and M. Carr (1995), Comparison of turbulence kinetic energy dissipation rate estiamtes from two ocean microstructure profilers, *J. Atmos. Ocean. Tech.*, *12*, 346–366.
Moum, J. N., and J. D. Nash (2009), Mixing Measurements on an Equatorial Ocean Mooring, *J. Atmos. Ocean. Tech.*, *26*, 317–336.
Moum, J. N., and T. P. Rippeth (2009), Do observations adequately resolve the natural variability of oceanic turbulence?, *J. Mar. Sys.*, *77*, 409–417.
Moum, J. N., R.-C. Lien, A. Perlin, J. D. Nash, M. C. Gregg, and P. J. Wiles (2009), Sea surface cooling at the equator by subsurface mixing in tropical instability waves, *Nature Geoscience*, *2*, 761–765.
Moum, J. N., J. D. Nash, and W. D. Smyth (2011), Narrowband oscillations in the upper equatorial ocean. part i: Interpretation as shear instabilities, *J. Phys. Ocean.*, *41*(3), 397–411.
Müller, P., and X. Liu (2000), Scattering of internal waves at finite topography in two dimensions. part I: Theory and case studies, *J. Phys. Oceanogr.*, *30*, 532–549.
Müller, P., G. Holloway, F. Henyey, and N. Pomphrey (1986), Nonlinear interactions among internal gravity waves, *Rev. Geophys*, *24*(3), 493–536.
Munk, W., and C. Wunsch (1998), Abyssal recipes II: Energetics of tidal and wind mixing, *Deep-Sea Res. Part I*, *45*, 1977–2010.
Munk, W. H. (1966), Abyssal recipes, *Deep-Sea Res.*, *13*, 707–730.
Nagasawa, M., N. Yoshihiro, and T. Hibiya (2000), Spatial and temporal distribution of the wind-induced internal wave energy available for deep water mixing in the north pacific, *J. Geophys. Res.*, *105*(C6), 13,933–13,943.
Nash, J. D., E. Kunze, J. M. Toole, and R. W. Schmitt (2004), Internal tide reflection and turbulent mixing on the continental slope, *J. Phys. Oceanogr.*, *34*, 1117–1134.
Naveira Garabato, A., K. Polzin, B. King, K. Heywood, and M. Visbeck (2004), Widespread intense turbulent mixing in the Southern Ocean, *Science*, *303*, 210–213.

Nikurashin, M., and R. Ferrari (2010), Radiation an ddissipation of internal waves generated by geostrophic motions impinging on small-scale topography: Application to the Southern Ocean, *J. Phys. Oceanogr.*, *40*, 2025–2042.

Nikurashin, M., and R. Ferrari (2011), Global energy conversion rate from geostrophic flows into internal lee waves in the deep ocean, *Geophys. Res. Lett.*, *38*, 10.1029/2011GL046,576.

Nikurashin, M., and S. Legg (2011), A mechanism for local dissipation of internal tides generated at rough topography, *J. Phys. Oceanogr.*, *41*, 378–395.

Nikurashin, M., and G. Vallis (2011), A theory of deep stratification and overturning circulation in the oce, *J. Phys. Oceanogr.*, *41*, 485–502.

Osborn, T. R. (1980), Estimates of the local rate of vertical diffusion from dissipation measurements, *J. Phys. Oceanogr.*, *10*, 83–89.

Pacanowski, R., and S. Philander (1981), Parameterization of vertical mixing in numerical models of tropical oceans, *J. Phys. Oceanogr.*, *11*(11), 1443–1451.

Palmer, M. D., A. C. N. Garabato, J. D. Stark, J. J.-M. Hirschi, and J. Marotzke (2007), The influence of diapycnal mixing on quasi-steady overturning states in the Indian Ocean, *J. Phys. Ocean.*, *37*, 2290–2304.

Peacock, T., P. Echeverri, and N. J. Balmforth (2008), An experimental investigation of itnernal tide generaiton by two-dimensional topography, *J. Phys. Oceanogr.*, *38*, 235–242.

Perlin, A., J. N. Moum, and J. M. Klymak (2005), Response of the bottom boundary layer over a sloping shelf to variations in alongshore wind, *J. Geophys. Res.*, *110*, doi:10.1029/2004JC002,500, submitted.

Pinkel, R., M. Buijsman, and J. M. Klymak (2012), Breaking Topographic Lee Waves in a Tidal Channel in Luzon Strait, *Oceanography*, *25*(2), 160–165.

Plueddemann, A. J., and J. T. Farrar (2006), Observations and models of the energy flux from the wind to mixed-layer inertial currents, *Deep-Sea Res.*, *53*, 5–30.

Pollard, R., and R. Millard (1970), Comparison between observed and simulated wind-generated inertial oscillations, *Deep-Sea Res.*, *17*, 153–175.

Polton, J., and S. Belcher (2007), Langmuir turbulence and deeply penetrating jets in an unstratified mixed layer, *J. Geophys. Res.*, *112*, doi:10.1029/2007JC004,205.

Polton, J. A., J. A. Smith, J. A. MacKinnon, and A. Tejada-Martinez (2008), Rapid generation of high-frequency internal waves beneath a wind and wave forced oceanic surface mixed layer, *Geophys. Res. Lett.*, *35*(L13602, doi:10.1029/2008GL033856).

Polzin, K. (2004), Idealized solutions for the energy balance of the finescale internal wave field, *J. Phys. Oceanogr.*, *34*, 231–246.

Polzin, K., and E. Firing (1997), Estimates of diapycnal mixing using LADCP and CTD data from I8S, *Int. WOCE Newslett*, *29*, 39–42.

Polzin, K., J. Toole, J. Ledwell, and R. Schmitt (1997), Spatial variability of turbulent mixing in the abyssal ocean, *Science*, *276*, 93–96.

Polzin, K. L. (2009), An abyssal recipe, *Ocean Modelling*, *30*, 298–309.

Polzin, K. L. (2010), Mesoscale Eddy–Internal Wave Coupling. Part II: Energetics and Results from PolyMode, *J. Phys. Oceanogr.*, *40*, 789–801.

Polzin, K. L., and Y. V. Lvov (2011), Toward regional characterizations of the oceanic internal wavefield, *Rev. Geophys.*, *49*, doi:10.1029/2010RG000,329.

Polzin, K. L., J. M. Toole, and R. W. Schmitt (1995), Finescale parameterizations of turbulent dissipation, *J. Phys. Oceanogr.*, *25*, 306–328.

Polzin, K. L., N. S. Oakey, J. M. Toole, and R. W. Schmitt (1996a), Fine structure and microstructure characteristics across the northwest Atlantic Subtropical Front, *J. Geophys. Res.*, *101*(C6), 14,111–14,121.

Polzin, K. L., K. G. Speer, J. M. Toole, and R. W. Schmitt (1996b), Intense mixing of Antarctic Bottom Water in the equatorial Atlantic Ocean, *Nature*, *380*, 54–57.

Polzin, K. L., A. C. N. Garabato, T. N. Huussen, B. M. Sloyan, and S. N. Waterman (2013), Finescale parameterizations of turbulent dissipation by internal wave breaking, *Rev. Geophys.*, *submitted*.

Price, J., J. Morzel, and P. Niiler (2008), Warming of sst in the cool wake of a moving hurricane, *J. Geophys. Res*, *113*, C07,010.

Price, J. F., R. A. Weller, and R. Pinkel (1986), Diurnal cycling: Observations and models of the upper ocean response to diurnal heating, cooling, and wind mixing, *J. Geophys. Res.*, *91*, 8411–8427.

Radko, T., and J. Marshall (2004), The leaky thermocline, *J. Phys. Oceanogr.*, *34*, 1648–1662.

Rainville, L., and R. Pinkel (2004), Observations of energetic high-wavenumber internal waves in the Kuroshio, *J. Phys. Oceanogr.*, *34*, 1495–1505.

Ray, R., and G. Mitchum (1996), Surface manifestation of internal tides generated near hawaii, *Geophysical Research Letters*, *23*(16), 2101–2104.

Ray, R., and G. Mitchum (1997), Surface manifestation of internal tides in the deep ocean: Observations from altimetry and island gauges, *Progress in Oceanography*, *40*(1), 135–162.

Roemmich, D., S. Hautala, and D. Rudnick (1996), Northward abyssal transport through the Samoan Passage and adjacent regions, *J. Geophys. Res.*, *101*, 14,039–14,055.

Rudnick, D., et al. (2003), From tides to mixing along the Hawaiian Ridge, *Science*, *301*, 355–357.

Rudnick, D. L., and R. Ferrari (1999), Compensation of horizontal temperature and salinity gradients in the ocean mixed layer, *Science*, *283*, 526–529.

Saenko, O., and W. Merryfield (2005), On the effect of topographically enhanced mixing on the global ocean circulation, *J. Phys. Oceanogr.*, *35*, 826–834.

Samelson, R. M. (1998), Large scale circulation with locally enhanced vertical mixing, *J. Phys. Oceanogr.*, *28*(4), 712–726.

Schmitt, R., J. Ledwell, E. Montgomery, K. Polzin, and J. Toole (2005), Enhanced diapycnal mixing by salt fingers int he thermoclin of the tropical Atlantic, *Science*, *308*(685-688).

Schmitt, R. W. (2012), Finger puzzles, *J. Fluid Mech.*, *692*, 1–4.

Scott, J. R., and J. Marotzke (2002), The location of diapycnal mixing and the Meridional Overturning Circulation, *J. Phys. Oceanogr.*, *32*, 3578–3595.

Scott, R. B., J. A. Goff, A. C. N. Garabato, and A. J. G. Nurser (2011), Global rate and spectral characteristics of internal gravity wave generation by geostrophic flow over topography, *J. Geophys. Res.*, *116*, 10.1029/2011JC007,005.

Shih, L. H., J. R. Koseff, G. N. Ivey, and J. H. Ferziger (2005), Paramteriztion of turbulent fluxes and scales using homogeneous sheared stably stratified turbulence simulations, *J. Fluid Mech.*, *525*, 193–214.

Shuckburgh, E., G. Maze, D. Ferreira, J. Marshall, H. Jones, and C. Hall (2011), Mixed layer lateral eddy fluxes mediated by air-sea interaction, *J.*

Phys. Oceanogr., *41*, 130–144.

Silverthorne, K. E., and J. M. Toole (2009), Seasonal kinetic energy variability of near-inertial motions, *J. Phys. Ocean.*, *39*(4), 1035–1049.

Simmons, H., S. Jayne, L. S. Laurent, and A. Weaver (2004a), Tidally driven mixing in a numerical model of the ocean general circulation, *Ocean Modelling*, *6*, 245–263.

Simmons, H. L. (2008), Spectral modification and geographic redistribution of the semi-diurnal internal tide, *Ocean Modelling*, *21*, 126–138.

Simmons, H. L., R. W. Hallberg, and B. K. Arbic (2004b), Internal wave generation in a global baroclinic tide model, *Deep-Sea Res II*, *51*, 3043–3068.

Skyllingstad, E. D., and E. D. Denbo (1995), An ocean large-eddy simulation of Langmuir circulations and convection in the surface mixed layer, *J. Geophys. Res.*, *100*, 8501–8522.

Skyllingstad, E. D., W. D. Smyth, and G. B. Crawford (2000), Resonant wind-driven mixing in the ocean boundary layer, *J. Phys. Oceanogr.*, *30*, 1866–1890.

Sloyan, B. M. (2005), Spatial variability of mixing in the Southern Ocean, *Geophys. Res. Lett.*, *32*, L18,603, doi:10.1029/2005GL023,568.

Smyth, W. D., and J. N. Moum (2001), Three-dimensional turbulence, in *Encyclopedia of Ocean Sciences*, vol. 6, pp. 2947–2955, Academic Press.

Smyth, W. D., and J. N. Moum (2012), Ocean Mixing by Kelvin-Helmholtz Instability, *Oceanography*, *25*(2), 140–149.

Smyth, W. D., J. N. Moum, and J. D. Nash (2011), Narrowband oscillations in the upper equatorial ocean. part ii: Properties of shear instabilities, *J. Phys. Oceanogr.*, *41*(3), 412–428.

St. Laurent, L., and C. Garrett (2002), The role of internal tides in mixing the deep ocean, *J. Phys. Oceanogr.*, *32*, 2882–2899.

St. Laurent, L., H. Simmons, and S. Jayne (2002), Estimating tidally driven mixing in the deep ocean, *Geophys. Res. Lett.*, *29*(23), doi:10.1029/2002GL015,633.e.

St. Laurent, L. C., and H. Simmons (2006), Estimates of power consumed by mixing in the ocean interior, *J. Climate*, *19*, 4877–4890.

St. Laurent, L. C., A. C, J. R. Ledwell, A. M. Thurnherr, J. M. Toole, and A. J. Watson (2012), Turbulence and diapycnal mixing in Drake Passage, *J. Phys. Oceanogr.*, *42*(12), 2143–2152, doi:10.1175/JPO-D-12-027.1.

Staquet, C., and J. Sommeria (2002), Internal gravity waves: from instabilities to turbulence, *Ann. Rev. Fluid Mech.*, *34*, 559–593.

St.Laurent, L. C., and A. M. Thurnherr (2007), Intense mixing of lower thermocline water on the crest of the Mid-Atlantic Ridge, *Nature*, *448*, 680–683.

St.Laurent, L. C., J. M. Toole, and R. W. Schmitt (2001), Buoyancy forcing by turbulence above rough topography in the abyssal Brazil Basin, *J. Phys. Oceanogr.*, *31*, 3476–3495.

Stommel, H., and A. Arons (1960), On the abyssal circulation of the world ocean—ii. an idealized model of the circulation pattern and amplitude in oceanic basins, *Deep Sea Research*, *6*, 217–233.

Stone, P. H. (1966), On non-geostrophic baroclinic stability, *J. Atmos. Sci.*, *23*(4), 390.

Stone, P. H. (1970), On non-geostrophic baroclinic stability 2, *J. Atmos. Sci.*, *27*(5), 721.

Sullivan, P., and J. McWilliams (2010), Dynamics of winds and currents coupled to surface waves, *Annual Review of Fluid Mechanics*, *42*, 19–42.

Sullivan, P., J. McWILLIAMS, and W. Melville (2004), The oceanic boundary layer driven by wave breaking with stochastic variability. part 1. direct numerical simulations, *Journal of Fluid Mechanics*, *507*, 143–174.

Talley, L. D. (2013), Closure of the global overturning circulation through the Indian, Pacific, and Southern Oceans: Schematics and transports, *Oceanography*, *26*(1), 80–97.

Talley, L. D., J. L. Reid, and P. E. Robbins (2003), Data-based meridional overturning streamfunctions for the global ocean, *J. Climate*, *16*(10), 3213–3226.

Talley, L. D., G. L. Pickard, W. J. Emery, and J. H. Swift (2011), *Descriptive Physical Oceanography: An Introduction*, 6th ed., Elsevier, Boston.

Tandon, A., and C. Garrett (1995), Geostrophic adjustment and restratification of a mixed-layer with horizontal gradients above a stratified layer, *J. Phys. Oceanogr.*, *25*(10), 2229–2241.

Taylor, J. R., and R. Ferrari (2010), Buoyancy and wind-driven convection at mixed layer density fronts, *J. Phys. Oceanogr.*, *40*, 1222–1242.

Thomas, L. N. (2005), Destruction of potential vorticity by winds, *J. Phys. Oceanogr.*, *35*, 2457–2466.

Thomas, L. N. (2012), On the effects of strain on symmetric instability and near-inertial motions, in review for JFM.

Thomas, L. N., and R. Ferrari (2008), Friction, frontogenesis, and the stratification of the surface mixed layer, *J. Phys. Oceanogr.*, *38*, 2501–2518.

Thomas, L. N., and J. R. Taylor (2010), Reduction of the usable wind-work on the general circulation by forced symmetric instability, *Geophys. Res. Lett.*, *37*(L18606), doi:10.1029/2010GL044,680.

Thompson, A. F., S. T. Gille, J. A. MacKinnon, and J. Sprintall (2007), Spatial and temporal patterns of small-scale mixing in Drake Passage, *J. Phys. Oceanogr.*, *37*, 572–592.

Thorpe, A. J., and R. Rotunno (1989), Nonlinear aspects of symmetric instability, *J. Atmos. Sci.*, *46*, 1285–1299.

Thorpe, S. (2005), *The turbulent ocean*, Cambridge Univ. Press.

Thurnherr, A. M., L. St. Laurent, K. Speer, J. Toole, and J. Ledwell (2005), Mixing sssociated with sills in a canyon in the midocean ridge flank, *J. Phys. Ocean.*, *35*, 1370–1381.

Timmermans, M., C. Garrett, and E. Carmack (2003), The thermohaline structure and evolution of the deep waters in the Canada Basin, Arctic Ocean, *Deep Sea Research Part I: Oceanographic Research Papers*, *50*, 1305–1321.

Toggweiler, J., and B. Samuels (1998), On the ocean's large-scale circulation near the limit of no vertical mixing, *J. Phys. Oceanogr.*, *28*(9), 1832–1852.

Toole, J. M., K. L. Polzin, and R. W. Schmitt (1994), Estimates of diapycnal mixing in the abyssal ocean, *Science*, *264*, 1120–1123.

Toole, J. M., R. W. Schmitt, K. L. Polzin, and E. Kunze (1997), Near-boundary mixing above the flanks of a midlatitude seamount, *J. Geophys. Res.*, *102*(C1), 947–959.

Treguier, A. M., I. M. Held, and V. D. Larichev (1997), On the parameterization of quasi-geostrophic eddies in primitive equation ocean models, *Journal of Physical Oceanography*, *27*, 567–580.

van Haren, H. (2007), Longitudinal and topographic variations in North Atlantic tidal and intertial energy around latitudes 30 ± 10 N, *J. Geophys. Res.*, *112*(doi:10.1029/2007JC004193).

Venayagamoorthy, S. K., and O. B. Fringer (2012), Examining Breaking Internal Waves on a Shelf Slope Using Numerical Simulations, *Oceanog-*

raphy, *25*(2), 132–139.

Watanabe, M., and T. Hibiya (2002), Global estimates of the wind-induced energy flux to inertial motions in the surface mixed layer, *Geophys. Res. Lett.*, *29*(8), 10.1029/2001GL014,422.

Waterhouse, A., et al. (2013), Global patterns of mixing from direct and indirect measurements of dissipation, in prep.

Waterman, S., A. C. N. Garabato, and K. L. Polzin (2013a), Internal waves and turbulence in the Antarctic Circumpolar Current, *J. Phys. Oceanogr.*, *in press*, doi:10.1175/JPO-D-11-0194.1.

Waterman, S., K. L. Polzin, A. C. N. Garabato, and K. L. Sheen (2013b), Suppression of internal wave breaking by lee wave - mean flow interactions in the Antarctic Circumpolar Current, *J. Phys. Oceanogr.*, *submitted*.

Whalen, C. B., L. D. Talley, and J. A. MacKinnon (2012), Spatial and temporal variability of global ocean mixing inferred from Argo profiles, *Geophys. Res. Lett.*, *39*(L18612), doi:10.1029/2012GL053196.

Wijesekera, H., L. Padman, T. Dillon, M. Levine, and C. Paulson (1993), The application of internal-wave dissipation models to a region of strong mixing, *J. Phys. Oceanogr.*, *23*, 269–286.

Wijesekera, J., and T. Dillon (1991), Internal waves and mixing in the upper Equatorial Pacific Ocean, *J. Geophys. Res.*, *96*, 7115–7125.

Winters, K., and E. D'Asaro (1994), Three-dimensional wave instability near a critical level, *J. Fluid Mech.*, *272*, 255–284.

Winters, K. B., and E. A. D'Asaro (1997), Direct simulation of internal wave energy transfer, *J. Phys. Oceanogr.*, *27*, 1937–1945.

Wolfe, C. L., and P. Cessi (2010), What sets the strength of the middepth stratification and overturning circulation in eddying ocean models?, *J. Phys. Oceanogr.*, *40*(7), 1520–1538.

Wolk, F., R. G. Lueck, and L. St. Laurent (2009), Turbulence measurements from a glider, in *OCEANS 2009, MTS/IEEE Biloxi - Marine Technology for Our Future: Global and Local Challenges.*, pp. 1–6.

Wunsch, C., and R. Ferrari (2004), Vertical mixing, energy and the general circulation of the oceans, *Ann. Rev. Fluid Mech.*, *36*, 281–412.

Young, K. (2012), Biogenic inputs to ocean mixing, *J. Exp. Bio*, *in press*.

Young, W., and M. Ben-Jelloul (1997), Propagation of near-inertial oscillations through a geostrophic flow, *J. Mar. Res.*, *55*, 735–766.

Zervakis, V., and M. Levine (1995), Near-inertial energy propagation from the mixed layer: theoretical considerations, *J. Phys. Oceanogr.*, *25*, 2872–2889.

Zhai, X., H. L. Johnson, and D. P. Marshall (2010), Significant sink of ocean-eddy energy near western boundaries, *Nature Geoscience*, *3*, 608–612.

Zhao, Z., and M. H. Alford (2009), New altimetric estimates of mode-one M2 internal tides in the Central North Pacific Ocean, *jpo*, *39*, 1669–1684.

Zhao, Z., M. H. Alford, J. A. MacKinnon, and R. Pinkel (2010), Long-range propagation of the semidiurnal internal tide from the Hawaiian Ridge, *J. Phys. Oceanogr.*, *40*(4), 713–736.

Zika, J. D., B. Sloyan, and T. J. McDougall (2009), Diagnosing the Southern Ocean overturning from tracer fields, *J. Phys. Oceanogr.*, *39*(11), 2926–2940.